

NETWORK NEURO SCIENCE

an open access  journal



Citation: Jüchtern, M., Shaikh, U. J., Caspers, S., & Binkofski, F. (2024). A gradient of hemisphere-specific dorsal to ventral processing routes in parieto-premotor networks. *Network Neuroscience*, 8(4), 1563–1589. https://doi.org/10.1162/netn_a_00407

DOI:
https://doi.org/10.1162/netn_a_00407

Supporting Information:
https://doi.org/10.1162/netn_a_00407

Received: 19 January 2024
Accepted: 6 June 2024

Competing Interests: The authors have declared that no competing interests exist.

Corresponding Author:
Ferdinand Binkofski
fbinkofski@ukaachen.de


Handling Editor:
Alex Fornito

Copyright: © 2024
Massachusetts Institute of Technology
Published under a Creative Commons
Attribution 4.0 International
(CC BY 4.0) license



RESEARCH

A gradient of hemisphere-specific dorsal to ventral processing routes in parieto-premotor networks

Marvin Jüchtern¹, Usman Jawed Shaikh¹, Svenja Caspers^{2,3,5*}, and Ferdinand Binkofski^{1,4,5*} 

¹Department of Clinical Cognition Science, Clinic of Neurology at the RWTH Aachen University Faculty of Medicine, ZBMT, Aachen, Germany

²Institute for Neuroscience and Medicine (INM-1), Research Centre Jülich GmbH, Jülich, Germany

³Institute for Anatomy I, Medical Faculty & University Hospital Düsseldorf, Heinrich-Heine-Universität Düsseldorf, Düsseldorf, Germany

⁴JARA-BRAIN, Juelich-Aachen Research Alliance, Juelich, Germany

⁵Institute for Neuroscience and Medicine (INM-4), Research Center Jülich GmbH, Jülich, Germany

*Both authors contributed equally as senior authors to this work.

Keywords: Dorsal stream, Frontoparietal, Graph theory analysis, Structural connectivity, Tractography

ABSTRACT

Networks in the parietal and premotor cortices enable essential human abilities regarding motor processing, including attention and tool use. Even though our knowledge on its topography has steadily increased, a detailed picture of hemisphere-specific integrating pathways is still lacking. With the help of multishell diffusion magnetic resonance imaging, probabilistic tractography, and the Graph Theory Analysis, we investigated connectivity patterns between frontal premotor and posterior parietal brain areas in healthy individuals. With a two-stage node characterization approach, we defined the network role of precisely mapped cortical regions from the Jülich-Brain atlas. We found evidence for a third, left-sided, medio-dorsal subpathway in a successively graded dorsal stream, referencing more specialized motor processing on the left. Supplementary motor areas had a strongly lateralized connectivity to either left dorsal or right ventral parietal domains, representing an action-attention dichotomy between hemispheres. The left sulcal parietal regions primarily coupled with areas 44 and 45, mirrored by the inferior frontal junction (IFJ) on the right, a structural lateralization we termed as “Broca’s-IFJ switch.” We were able to deepen knowledge on gyral and sulcal pathways as well as domain-specific contributions in parieto-premotor networks. Our study sheds new light on the complex lateralization of cortical routes for motor activity in the human brain.

AUTHOR SUMMARY

Human motor abilities are processed via specialized yet intertwined pathways in the parietal and premotor cortex. These can be parcellated into networks of brain areas, sharing connection patterns that differ between hemispheres. We differentiated a set of graded pathways, connecting definable network hubs. The well-known Dorsal Stream for visuomotor transformation appears to be left-dominantly divisible into three distinct substreams, providing more anatomical detail about its specialization into visual and semantic segments. Supplementary motor areas show lateralized couplings with left

dorsal and right ventral parietal areas, respectively, while left-sided AIPS connectivity to area 44/45 is mirrored by right-sided intersulcal links to the inferior frontal sulcus, both deepening our understanding of incorporated multi-task faculties like attention and speech.

INTRODUCTION

Brain regions in the human frontal and parietal cortices process abilities that allow us to interact with our environment, arranged in functionally specific and structurally overlapping networks.

Visuomotor transformation:
The ability of the brain to use visual information from the environment for steering object interaction like reaching.

These abilities include skills like praxis, visuomotor transformation (Jeannerod et al., 1995), attention (Corbetta & Shulman, 2002; Thiebaut de Schotten, Dell'Acqua, et al., 2011), working memory, language (Saur et al., 2008), and tool use (Orban & Caruana, 2014), particularly serving the realization of target-directed movements (Sakreida et al., 2016; Verhagen et al., 2013). Basic principles for segregated circuits of parieto-premotor communication were first established through histological tracing and electrical stimulation in nonhuman primate brains (Rizzolatti & Luppino, 2001; Rizzolatti et al., 1998). It was proven that information travels between specialized, often complementary parietal and frontal areas, for instance, the ventral and dorsal stream (Rizzolatti & Matelli, 2003). The essential idea was that the posterior parietal cortex (PPC) receives input for different sensory modalities. Depending on the activation onset and intensity, specific projections dominate outgoing signals to, among others, premotor domains (Rizzolatti & Luppino, 2001; Rizzolatti et al., 1998). Hence, areas in the PPC and premotor cortex (PMC) function as places of integration and transformation, allowing for stimulus-adjusted action.

With the help of structural and functional brain imaging, individual cortical areas have been associated with distinct human abilities. In the current study, we were focusing on parietal and premotor association brain areas, which form a key network for movement processing and its supportive faculties.

Broca's area (area 44, area 45) in the ventrolateral prefrontal cortex (VLPFC) is well-known for its role in language (Saur et al., 2008), which is realized through a complex network of mainly left lateralized brain regions, like the adjacent inferior frontal sulcus (IFS) (Bradler, 2015) and the inferior frontal junction (IFJ) (Friederici & Gierhan, 2013). Furthermore, areas 44 and 45 are associated with object identity (Rottschy et al., 2012), movement analysis (Binkofski et al., 2000), and motor programs (Ramayya et al., 2010). While the IFS is also responsible for working memory and cognitive tasks (Bradler, 2015; Van Doren et al., 2010), the more caudal IFJ appears important for attention (Zanto et al., 2010) and cognitive control (Friederici & Gierhan, 2013).

The core PMC in humans comprises a ventral premotor cortex (PMv), usually associated with working memory (Liu & Pleskac, 2011) and motor planning (Nuttall et al., 2018), especially for grasping movements (Tomassini et al., 2007), as well as a dorsal portion (PMd), known to be engaged in cognition (Genon et al., 2017), reaching, and hand movements (Caspers et al., 2010).

Most dorsally, the supplementary motor area (SMA) is composed of an SMAproper and a PreSMA subregion, dealing with language (through ventral connectivity) (Hertrich et al., 2016), motor learning, planning and execution (Genon et al., 2017), as well as action timing (Passingham & Lau, 2019).

The PPC can be divided into an inferior and superior parietal lobule (IPL, SPL), separated by an anterior and posterior portion of the intraparietal sulcus (aIPS, pIPS). It is important to mention that the terms “AIP” and “PIP” are also used for more distinct subareas of the intraparietal sulcus (IPS) in macaque monkeys (Orban et al., 2006) and should not be confused with our current division of the human IPS into an anterior (aIPS) and a posterior (pIPS) segment.

While most of the IPL is active during attention tasks (Binkofski, Klann, & Caspers, 2016; Caspers et al., 2011; Corbetta & Shulman, 2002), language (Binkofski et al., 2016; Caspers et al., 2013), motor preparation, and planning of gestures, often for tool use (Caspers et al., 2011; Ramayya et al., 2010), especially areas in the supramarginal gyrus are putatively relevant for the mirror neuron system (Rizzolatti & Craighero, 2004) and coding of near-body objects (Brozzoli et al., 2011).

Both the aIPS and the pIPS are involved in attentional processes (Gillebert et al., 2013), while the former also shares information for reaching (Rodríguez-Herreros et al., 2015) and the latter is rather known for its involvement in arm/eye movement control (Konen et al., 2013) and language skills (Richter et al., 2019). Similarly, superior parietal hubs got associated with the processing of attention (Roski et al., 2013) and reaching movements (Diedrichsen et al., 2005).

It is important to note that many of these faculties are highly lateralized in the human brain, such as praxis in the left hemisphere (Jeannerod et al., 1995), musical processing in the right IFS (Bradler, 2015), word listening in the left IPL, and nonlinguistic listening in the right SMA (Hesling et al., 2019). Since hemispheric lateralization plays only a marginal role in the non-human primate cortex (Passingham, 2008), it becomes evident that segregated and graded cortico-cortical pathways must serve important purposes for complex, multitask behavior in humans.

Another key feature of the human-environment interaction is the visuomotor transformation for object interaction. It is known to be processed along integrated, but separate, dorsal substreams, that is, a dorso-dorsal and ventro-dorsal pathway (Binkofski & Buxbaum, 2013; Rizzolatti & Matelli, 2003), tracing back to the two-stream model of visual processing in nonhuman primates (Mishkin & Ungerleider, 1982) and humans (Goodale & Milner, 1992), which was very recently extended by a third, lateral pathway, involved mainly in social cognition aspects of visual processing (Pitcher & Ungerleider, 2021). While online action control happens mainly dorso-dorsally along the SPL and dorsal premotor domains, the ventro-dorsal stream (including aIPS, IPL, and PMv) serves more semantic aspects of space perception and action understanding (Binkofski & Buxbaum, 2013; Rizzolatti & Matelli, 2003). These features enable humans not only to use tools in a proper manner but also to cognitively process interaction and consciously observe the behavior of others (Orban & Caruana, 2014). For such multilayered processing of sensory perception, conceiving, and (re)active output coordination, integrated cortical circuits are necessary.

Consequently, in the current study, we aimed at getting a deeper understanding of connectivity lateralization and network contribution of posterior parietal and premotor brain areas. We therefore used the recently proposed, finely parcellated regions of interest (ROIs) from the Julich-Brain atlas (Amunts et al., 2020) and applied a de novo two-stage procedure for characterizing these areas as nodes in the respective networks. High-resolution diffusion-weighted magnetic resonance imaging (DW-MRI), probabilistic tractography, and Graph Theory Analysis (GTA) allowed us to depict the shortest paths of parieto-premotor couplings, located on segments of larger interlobar routes. We expected regionally specialized cortical circuitries, including functionally relevant differences between the two hemispheres and

Probabilistic tractography:
Method of fiber-tracking between regions of interest, where every connection is computed multiple times to improve certainty of a tract.

Graph Theory Analysis:
Set of mathematical tools used to analyze (brain) networks, abstracted into matrices of nodes (areas) and edges (links).

between segments of network pathways, representing the complexity of human multitask processing.

MATERIALS AND METHODS

Subjects

The current study included 40 right-handed healthy adults (21 females and 19 males, aged 20 to 62 years, median: 23.5 years, average: 25.0 years, standard deviation (*SD*): 7.0 years) who were recruited through advertising on campus. All subjects had no history of neurological disease and brain or heart surgery. Informed consent was obtained from each participant before the experiment. The study protocol was approved by the RWTH Aachen University Independent Ethics Committee (EK 077/16). All experiments were performed in accordance with the guidelines of the Declaration of Helsinki.

MRI Acquisition

All scans were performed on a Siemens MAGNETOM Prisma 3 Tesla MRI scanner (Siemens Medical Systems, Erlangen, Germany). Participants were instructed to lie calmly and move as little as possible during the measurement. A 20-channel head coil was used. High-resolution T₁-weighted images were obtained by magnetization prepared rapid-acquisition gradient echo sequences with parameters as follows: 1.0-mm slice thickness with no interslice gap, 192 slices, time repetition (TR) = 1,900 ms, echo time (TE) = 2.21 ms, time to inversion = 900 ms, number of excitations (NEX) = 1, in-plane acquisition matrix = 256 × 256, time of acquisition (TA) = 4:18 min.

Diffusion tensor images were acquired using a single-shot Echo-planar imaging-based sequence: whole-brain coverage, 1.5-mm slice thickness with no interslice gap, 92 axial slices, TR = 3,230 ms, TE = 89.2 ms, NEX = 1, in-plane acquisition matrix = 140 × 140 with 75% phase partial Fourier, FOV = 210 × 210 mm², TA = 5:41 min. We applied 99 diffusion directions with b-values = 0, 1,500 and 3,000 s/mm² in terms of a multishell acquisition scheme to benefit from a stronger MRI signal of a lower b-value as much as higher angular contrast of a larger b-value to obtain more accurate local fiber estimations (Jbabdi et al., 2012).

Preprocessing and Tractography

All preprocessing steps were executed in FSL (FMRIB's Software Library, version 6.0, URL: <https://fsl.fmrib.ox.ac.uk/fsl/fslwiki>). To correct for susceptibility-induced distortions, we applied the topup function (Andersson et al., 2003; Smith et al., 2004). Nonbrain tissue was removed via the BET tool (Smith, 2002). Distortion correction of eddy currents and subject head motion was conducted using the eddy tool (Andersson & Sotiropoulos, 2016).

For registration, the respective T1-weighted image was co-registered to the corresponding b = 0 image in the diffusion MRI space, using the FLIRT tool (Jenkinson et al., 2002; Jenkinson & Smith, 2001). On the newly created T1/b0 image, an inverse transformation was applied to warp the Julich-Brain atlas masks from the Montreal Neurological Institute (MNI) space to the diffusion MRI native space. The ROIs in this atlas were created probabilistically from a set of postmortem brain samples, merged into a whole-brain template, where, for each voxel, the probability of all cytoarchitectonic brain areas was considered to determine the most probable assignment (Eickhoff et al., 2005).

On the preprocessed diffusion data, we applied the BedpostX function (Hernández et al., 2013), using a multishell ball and zeppelins deconvolution (Sotiropoulos et al., 2016) as well

Multishell diffusion MRI:
Combining different b-values
(gradient strengths) in diffusion
magnetic resonance imaging
acquisition to enhance the
distinction of brain tissues.

as a Rician noise model instead of default Gaussian noise (Ibabdi et al., 2012). The output was used in probabilistic tractography via Probtrackx (Behrens et al., 2007).

In Probtrackx, we used a multiple-mask approach with 5,000 individual samples (i.e., streamlines) drawn from the center of each voxel. A symmetric ROI-by-ROI connectivity matrix was generated for all 37 brain areas, where each cell contains the probabilistic number of tracks seeded from a certain ROI, reaching another ROI. Anonymized connectivity matrices for all participants can be found as shared data in an open repository (DOI: 10.6084/m9.figshare.21814770).

The anatomical location of the network's ROIs can be found in Figures 1.1 and 1.2 in the MNI space. Please note that a depiction of the right hemisphere network was omitted due to its highly similar topography to avoid redundancy.

Please also find the comprehensive overview on the network's ROIs in the Supporting Information: A schematic overview on the network's anatomy is given as Supporting Information Figure S1. Centers of gravity for bilateral ROIs are presented in Supporting Information Table S1; size and corresponding cortical areas in nonhuman primates for the network's ROIs can be found in Supporting Information Table S2.

Prior to registration, the PMv ROI was manually created based on previous parcellation schemes for the human ventral PMC (cf., e.g., Callan et al., 2010). The left PMv had a centroid of $-45.91, -5.64, 42.34$ (x, y, z) and right PMv of $42.34, -5.70, 43.97$.

Postprocessing

Normalization of matrices was realized by division through the total number of generated tracts from a given seed in each subject (the so-called "waytotal"), as well as averaging by taking the mean of every (directional) ROI pair (i.e., a fronto-parietal and a parieto-frontal orientation). Our graph can therefore be classified as weighted-undirected because it contains edge weights (the probabilistic streamline count per link) and does not differentiate between

ROI parcellation:
Division of the brain into distinct areas of interest, using microanatomical parameters to define borders.

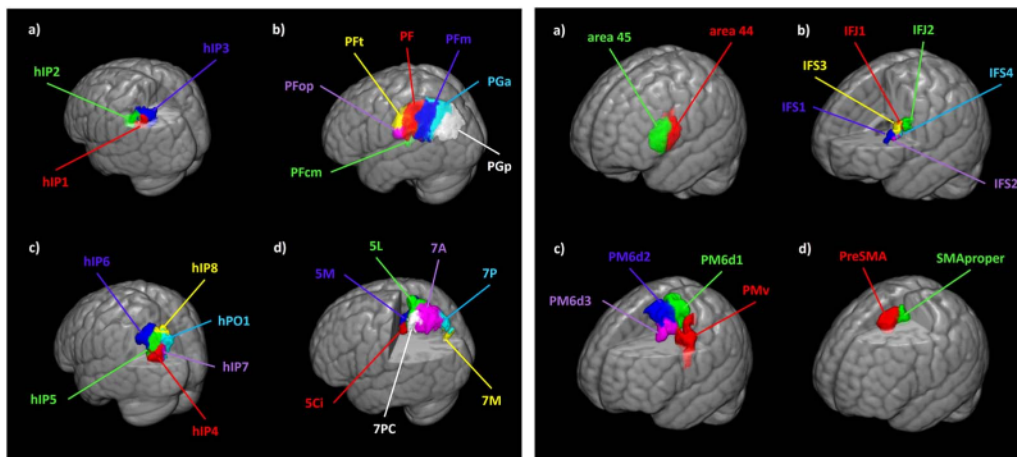


Figure 1. Localization of parietal ROIs in MNI space, left hemisphere. 1.1. Left-sided parietal ROIs on a three-dimensional brain template in MNI space. (A) aIPS: hIP1 (red), hIP2 (green), and hIP3 (blue). (B) IPL: PF (red), PFcm (green), PFm (blue), PFop (purple), PFt (yellow), PGa (light blue), and PGp (white). (C) pIPS: hIP4 (red), hIP5 (green), hIP6 (blue), hIP7 (purple), hIP8 (yellow), and hPO1 (light blue). (D) SPL: 5Ci (red), 5L (green), 5M (blue), 7A (purple), 7M (yellow), 7P (light blue), and 7PC (white). Localization of premotor ROIs in MNI space, left hemisphere. 1.2. Left-sided premotor ROIs on a three-dimensional brain template in MNI space. (A) VLPFC: area 44 (red) and area 45 (green). (B) IFS: IFJ1 (red), IFJ2 (green), IFS1 (blue), IFS2 (purple), IFS3 (yellow), and IFS4 (light blue). (C) PMC: PMv (red), PM6d1 (green), PM6d2 (blue), and PM6d3 (purple). (D) SMA: PreSMA (red) and SMAproper (green).

afferent and efferent paths. Since binarization can be considered as oversimplifying and the probability of molecular displacement along a vector is thought to be the same no matter the direction on the vector, this graph type is often recommended (Yeh et al., 2021). Note that only parieto-premotor couplings (i.e., 23 parietal \times 24 premotor = 322 ROIs) were included in the final analysis, omitting intralobular, local connections, which would have distorted the fronto-parietal connectivity analysis.

GTA tools facilitate the quantification of network properties by applying summary metrics (Rubinov & Sporns, 2010). In general, ROIs are called nodes (or vertices), while the connections between them, that is, the streamlines, are called edges (or links) of the graph. We used tools provided by the Brain Connectivity Toolbox (BCT; URL: <https://www.brain-connectivity-toolbox.net>) (Rubinov & Sporns, 2010).

In probabilistic connectomics, thresholding is a common tool for reducing weak connection weights as putative false positives in a network. Although a universally ideal threshold does not exist, most approaches decide for applying a specific range of thresholds to increase specificity of tractography data (Yeh et al., 2021). This multithreshold approach usually suggests a lower cutoff above 0.01 (normalized and averaged streamline count), since it seems adequate to include smaller but supposedly relevant long-distance couplings (Tsai, 2018). We decided for a two-step strategy where we first averaged all edge weights into a three-dimensional whole-group matrix ($\text{mean}(P_{ij}) + 2 \times SD(P_{ij})$, where SD is the standard deviation and P_{ij} is an edge of the graph), on which we secondly applied a threshold range between 0.01 and 0.1 in steps of 0.0025, resulting in 37 thresholded matrices per hemisphere (Cao et al., 2013; Tsai, 2018).

For validation of adequacy of the used threshold range, we exerted three goodness criteria proposed by Yun and colleagues (2020): (a) connectedness, (b) modularity, and (c) small-worldness. By that, we ensured that the selected thresholded graphs (a) only contain nodes that remain connected to other nodes in the network, (b) can be internally well divided into smaller subnetworks (i.e., modules), and (c) provide clear segregative and integrative features as a network.

Firstly, all thresholded graphs were screened for connectedness. Please find the respective MATLAB formula within the Supporting Information as Supplementary Methods (MATLAB, MathWorks, Version 2019b, URL: <https://www.mathworks.com/products/matlab.html>). An undirected graph is connected if every pair of nodes is linked by a path (of one or more edges).

Secondly, the modularity of all graphs was examined using Newman's spectral reordering algorithm (Newman, 2006), which is defined as:

$$Q = \frac{1}{l} \sum_{i,j \in N} \left(a_{ij} - \frac{k_i k_j}{l} \right) \delta_{m_i, m_j},$$

where m_i is a module containing node i and $\delta_{m_i, m_j} = 1$ if $m_i = m_j$, otherwise 0. A_{ij} stands for an element of the adjacency matrix, which becomes 1 if there is an edge between nodes i and j ; l represents the number of edges in the graph, and k is a node's degree.

As indicated in the Yun study, thresholded matrices with a maximized modularity "Q" of above 0.3 were supposed to be included, so that a high level of topological clustering was ensured.

Thirdly, it was tested if all thresholded graphs had a small-world topology. In short, a network is small-world if it combines functionally specialized modules (high segregation) and a robust number of intermodular links (high integration), while it appears to be more clustered

Small-worldness:

Feature of a network, having most of its components densely linked to each other with primarily short paths between them.

than random networks (Uehara et al., 2014). For evaluation of “small-worldness,” the clustering coefficient (CC) as well as the characteristic path length (CPL) were computed on native and null model networks for each threshold. The CC is given as follows (Watts & Strogatz, 1998):

$$C = \frac{1}{n} \sum_{i \in N} C_i = \frac{1}{n} \sum_{i \in N} \frac{2t_i}{k_i(k_i - 1)},$$

with C_i as the CC of node i ($C_i = 0$ for $k_i < 2$). The CPL is given as follows (Watts & Strogatz, 1998):

$$L = \frac{1}{n} \sum_{i \in N} L_i = \frac{1}{n} \sum_{i \in N} \frac{\sum_{j \in N, j \neq i} d_{ij}}{n - 1},$$

with L_i as the average distance between node i and the rest of nodes.

Ideally, the CC would have a value above 1, while the CPL is approximately 1 (Gong et al., 2009). In Humphries and Gurney (2008), small-worldness was stated as:

$$S = \frac{\frac{C}{C_{rand}}}{\frac{L}{L_{rand}}} \gg 1,$$

where C stands for the CC and L for the CPL.

Every matrix with a quotient above 1 was classified as small-world and included in further analysis (Uehara et al., 2014). The thresholded connectivity matrices for both hemispheres can be accessed via an open repository (DOI: 10.6084/m9.figshare.21378246).

We used the distance matrix function by Dijkstra’s algorithm, which contains lengths of shortest paths between all pairs of nodes, to find important couplings between ROIs across the network (Dijkstra, 1959). For connectivity analysis, an average of each ROI-to-ROI connection (link) across subjects was used ($\text{mean}(P_{ij}) + 2 \times SD(P_{ij})$). Focusing on the fronto-parietal connectivity, we counted all connection weights below the first quartile (25th percentile) as highly linked. This is because higher probabilistic streamline counts are equivalent to shorter path lengths between nodes, interpreted as high connectivity. Since length weights differ relatively little between neighboring brain regions, we added a second, more rigorous cutoff to detect strongest links below the 15th percentile. Note that thresholding had a marginal effect on distance matrix outcomes, so we refrained from comparing different threshold levels of distance matrices to each other, only using the threshold level with highest density in both hemispheres (i.e., 0.01). Distances matrices can be accessed via an open repository (DOI: 10.6084/m9.figshare.21814827).

Statistics

To examine connectivity data for statistical robustness between hemispheres, we applied a two-tailed paired-sample t test on each normalized and averaged parieto-premotor ROI-to-ROI connection ($n = 322$) across all 40 subjects. Links between ROIs were regarded significantly different between hemispheres to a significance level of $\alpha = 0.05$, corrected for multiple comparisons with the help of Benjamini-Hochberg’s false discovery rate (FDR) (Benjamini & Hochberg, 1995) to adjust for an elevated type I error rate, using an open-source calculation tool (Hemmerich, 2016). p values for all tracts can be found as Table 1 in the Results section.

Furthermore, to add information on the variability of the obtained data, we calculated the coefficient of variation (CV), which is the SD divided by the mean, for each connection ($n =$

Distance matrix:
Algorithm where strong connection
between two areas is defined as
fewer steps between them.

Table 1. FDR-corrected p values for two-sided paired-sample t tests of connections between hemispheres

	Area 44	Area 45	IFJ1	IFJ2	IFS1	IFS2	IFS3	IFS4	PM6d1	PM6d2	PM6d3	PMv	PreSMA	SMA
hiP1	0.0023667	< 0.001	< 0.001	0.0469326	< 0.001	< 0.001	< 0.001	0.0010039	0.0024258	0.1104164	0.0487397	0.00348	0.8156032	0.3617242
hiP2	0.7974269	< 0.001	0.0204809	0.4950802	0.0073117	0.0020621	0.0069286	0.0028764	0.0561434	0.5565783	0.1897719	0.4499954	0.0892199	0.0274688
hiP3	0.0033756	< 0.001	0.0010039	0.2422001	< 0.001	< 0.001	< 0.001	0.0020621	0.0774355	0.1071989	0.1341073	< 0.001	0.3658591	0.4687232
PF	0.3185675	< 0.001	0.2197666	< 0.001	0.1313365	0.1707387	0.727806	0.9235359	0.7041408	0.0386906	0.0784085	< 0.001	0.0176156	0.9255557
PFcm	0.0029976	0.1045335	0.6098173	0.191486	0.9171359	0.4089526	0.7296598	0.1362293	0.7227876	0.002706	0.3504614	0.0500386	0.0016353	0.7107162
PFm	0.0021032	< 0.001	< 0.001	0.4942678	< 0.001	0.0020656	< 0.001	< 0.001	0.1712998	0.4982229	0.2197709	0.0992454	0.8804458	0.9070918
PFop	0.1578298	< 0.001	0.4942678	0.2033618	0.0973239	0.5352669	0.4799583	0.8661893	0.075838	0.1660618	0.5352669	0.1675581	0.0387771	0.0892199
Pft	0.0191359	< 0.001	0.8970892	0.013592	0.0028808	0.0081328	0.0509773	0.1176283	0.8991613	0.1707387	0.371324	0.042167	0.0023512	0.1686857
PGa	0.0163172	< 0.001	< 0.001	0.0315038	< 0.001	< 0.001	< 0.001	< 0.001	0.005143	0.1013966	0.0091531	0.0073699	0.5352669	0.2800028
PGp	0.9061361	< 0.001	0.0140144	0.2271843	0.0022664	0.0022145	0.0158101	0.0050797	0.0254012	0.0315038	0.2180517	0.001057	0.0236757	0.8970892
hiP4	0.9316835	0.0016353	0.0552704	0.22447	0.0140144	0.0609537	0.0152229	0.0500386	0.5352669	0.851328	0.7041408	0.0522232	0.8967706	0.2828541
hiP5	0.8526877	0.0042671	0.0246467	0.2271843	0.0466256	0.1362293	0.0152229	0.1015147	0.8890855	0.3504614	0.8298811	0.0063892	0.4499954	0.4917031
hiP6	0.0712709	0.0010499	0.01874	0.1678734	0.0039496	0.0264552	0.0138279	0.0366764	0.0267857	0.1039426	0.4089526	< 0.001	0.1362293	0.3088498
hiP7	0.0650695	< 0.001	0.0505421	0.157047	0.0269179	0.0199261	0.0152229	0.0325067	0.0200141	0.1712998	0.0509046	0.0325067	0.4563544	0.1131812
hiP8	0.967657	< 0.001	0.1161571	0.7608467	0.1039426	0.2281722	0.0466256	0.2580848	0.7041408	0.1882006	0.8701597	0.0892199	0.1176283	0.4068486
PO1	0.074198	< 0.001	0.4089526	0.7041408	0.1755293	0.3104376	0.153504	0.382507	0.3845758	0.1897719	0.8986166	0.2433916	0.0387771	0.3719002
SC1	0.1176283	0.5452344	0.5097973	0.1126345	0.5251358	0.1871689	0.9127906	0.0756063	0.0569304	0.00248	0.0158101	0.0020621	0.0011791	0.1383248
5L	0.0509773	< 0.001	0.1878175	0.4865146	0.0081328	0.0073117	0.0254012	0.6148503	0.0715968	0.9661052	0.4982229	< 0.001	0.2691185	0.8724889
5M	0.3139977	0.1898064	0.7296598	0.8915714	0.8890855	0.6925735	0.3860333	0.2710402	0.0340475	0.1050867	0.7702203	0.078014	0.0061126	0.0033286
7A	0.5352669	< 0.001	0.0028269	0.4687232	0.0069286	0.0048431	0.0073867	0.0412743	0.0010039	0.0010862	0.5352669	0.0257764	< 0.001	0.0061126
7M	0.6388747	0.0123777	0.0734867	0.6956897	0.0259424	0.0102898	< 0.001	0.2676772	0.0315038	0.0234693	0.0073117	0.2525939	0.4206409	0.2691185
7PC	0.0054723	< 0.001	0.0062065	0.8970892	< 0.001	< 0.001	< 0.001	< 0.001	0.0014	0.001288	0.0140055	< 0.001	< 0.001	0.0069286
7P	0.7088634	< 0.001	0.0158101	0.5352669	0.0715968	0.0810926	0.0023727	0.0840798	0.8382244	0.011362	0.7124653	< 0.001	< 0.001	0.0033286

$N = 322$ two-sided paired-sample t tests, adjusted for elevated type I errors by FDR correction with a significance level of $\alpha = 0.05$. p values for tracts between frontal (columns) and parietal (rows) ROIs across all 40 participants. Cells with light green background have a p value greater than 0.05. p values lower than 0.001 are written “<0.001” due to computational reasons.

322) in the two hemispheres across participants. To determine tracts with similar variability in the network, we applied a quartile clustering to the *SD* matrices of both hemispheres. The lowest *SD*s, below the first quartile of CV values in the hemisphere, were labeled as cluster A. Clusters B and C summarized tracts with an CV value below the second and third quartile, respectively. The highest CV values were grouped in cluster D. Complete CV matrices are obtainable as Supporting Information Figures S2.1 and S2.2.

Node Characterization

Regarding network nodes, we propose a novel design for hub identification and characterization. It is based on principles of node centrality, while a “hub” is defined as a node with high centrality whatsoever. Centrality is the property of a node to interact with other nodes and thereby shape a network’s integration (Rubinov & Sporns, 2010). We usually differentiate individual aspects of centrality, such as degree (centrality), which describes the amount of neighboring links a node has (again distinguished between within-module and between-module connectivity), and betweenness centrality, which quantifies how often a node is located on a shortest path between a pair of nodes in the network (Rubinov & Sporns, 2010).

We suggest a two-stage classification approach to define the specific role of brain regions in a network. For a schematic visualization, see Figure 2; for a detailed discussion of our approach and its interpretation, see the Supplementary Discussion at the Supporting Information. At the first stage, we used two functions to define network hubs: participation coefficient (PC) and within-module degree z-score (WMDZ).

The PC quantifies the portion of intermodular connectivity for a given node by using the community affiliation vector from a modularity function (Guimerà & Nunes Amaral, 2005). Since it displays the distribution of node connections among different modules, higher values of PC define “connector hubs” (or “intercluster hubs”), serving as bridges between separate clusters of nodes.

An exact description of the PC is given as follows (Guimerà & Nunes Amaral, 2005):

$$y_i = 1 - \sum_{m \in M} \left(\frac{k_i(m)}{k_i} \right)^2,$$

defining M as the set of modules (provided by modularity) and $k_i(m)$ as the number of links between i and all nodes in module m .

The WMDZ is the within-module version of degree centrality in a given network and is typically associated with “provincial hubs” (or “intracluster hubs”) (Cohen & D’Esposito, 2016; Rubinov & Sporns, 2010) that link vertices within a single cluster. In the same article, we find the mathematical definition of the WMDZ (Guimerà & Nunes Amaral, 2005):

$$z_i = \frac{k_i(m_i) - \bar{k}(m_i)}{\sigma^{k(m_i)}},$$

with m_i as a module containing node i , $k_i(m_i)$ as the within-module degree of i , $\bar{k}(m_i)$ as the mean, and $\sigma^{k(m_i)}$ as the *SD* of the within-module m_i degree distribution.

By means of these two functions, we were able to classify nodes as either connector hubs (PC > third quartile in at least the highest and lowest threshold of all networks), provincial hubs

Betweenness centrality:
Fraction of shortest paths that pass through a certain area (node) or tract (edge), serving high information flow.

Network hub:
Brain area with many (local or distant) interconnections, collecting multiple pathways as a crossing point in a network.

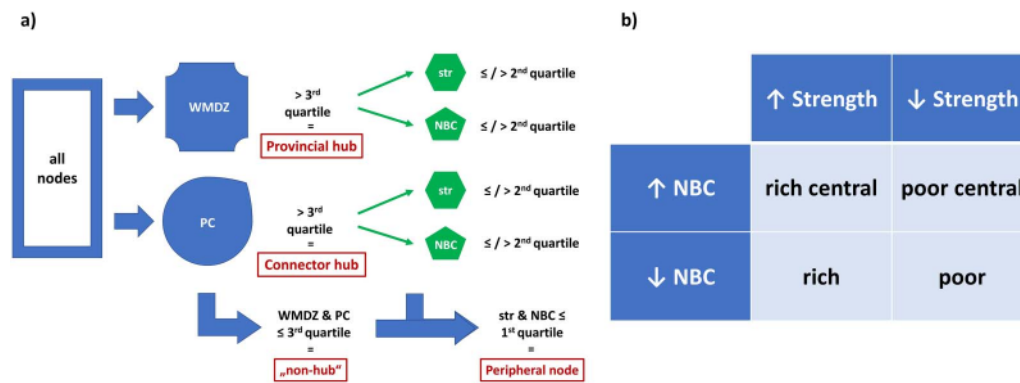


Figure 2. Node character assignment. (A) Every node was tested for hub status and type using WMDZ and PC. Hubs were further subclassified by strength (str) and NBC, while nonhubs were either called peripheral or remained unassigned. (B) Hub characterization depending on strength and NBC; “↑” means > second quartile, “↓” means ≤ second quartile.

(WMDZ > third quartile in at least the highest and lowest threshold of all networks), or non-hubs, with the latter failing both criteria. We did not include hubs in the final classification that lay above the PC/WMDZ cutoff only in occasional threshold graphs.

On the second stage, identified hubs were further differentiated and characterized by their degree and betweenness centrality, using two more graph theoretical tools from the BCT.

In weighted networks, the degree of a node is equivalent to its strength, which is the sum of weights of all edges linked to this node and highly proportional to its size (Farahani et al., 2019). Nodes with high strength (and relatively low betweenness) can be related to dense local connectivity, having rich input from the surrounding brain regions.

Node betweenness centrality (NBC) yields the fraction of all shortest paths in the network that contain a certain node, using the Brandes’ algorithm on connection-length matrices (Brandes, 2001). Freeman (1979) described the betweenness function in detail:

$$b_i = \frac{1}{(n-1)(n-2)} \sum_{\substack{h,j \in N \\ h \neq i, j \neq i}} \frac{\rho_{hj}(i)}{\rho_{hj}},$$

where ρ_{hj} is the number of shortest paths between h and j , and $\rho_{hj}(i)$ is the number of shortest paths between h and j passing through i .

A high NBC means that a node shares many shortest paths in a network and is therefore in a topographically strategic position, either locally or between separate modules.

As a result, we computed strength and NBC for all nodes formerly defined as hubs by PC or WMDZ and prefixed them with a more concise nodal property, summarized in Figure 2. NBC matrices and strength tables can be found in an open repository (DOI: 10.6084/m9.figshare.21814902; DOI: 10.6084/m9.figshare.21814917). Additionally, nonhubs with strength and NBC values below the first quartile in the given network were called “peripheral nodes” (also cf. Guimerà & Nunes Amaral, 2005; Meunier et al., 2009); the remaining nodes went unclassified.

RESULTS

Left Hemisphere Connectivity

Using a cytoarchitectonic parcellation from the Julich-Brain atlas, we were able to describe connecting paths between 37 ROIs in fronto-parietal networks. Results from probabilistic tractography were interpreted with the help of GTA. For quantitative analysis of tractography outcomes, we applied Dijkstra's distance matrix to the normalized and averaged connectivity matrices, including only parieto-premotor connections (i.e., 23 parietal \times 14 premotor = 322 ROIs), representing shortest paths of streamlines passing through pairs of ROIs; for detailed results, see Tables 2 and 3. Paired-sample *t* tests ($\alpha = 0.05$) were conducted on all ROI-to-ROI connections between hemispheres with *p* values FDR-corrected to control for statistical significance.

The largest patterns of connected ROIs on the left include an aIPS-area 44-Premotor group as well as an SPL-Premotor-SMA group; while in the right hemisphere, the former changed to aIPS-IFJ-Premotor connectivity and the latter toward IPL-areas plus human Intraparietal Area 6 (hIP6) connected to IFJ and PMC.

In detail, inferior frontal areas were well-linked to all aIPS and some IPL areas. While area 44 showed most parietal connections, especially with hIP6, 5M, 7A, and 7PC, left area 45 and IFJ2 resembled each other in having strong connections to aIPS, PFm, and PGa. IFS areas as well as IFJ1 primarily linked to parts of the aIPS, which we called intersulcal connections, in contrast to gyro-sulcal connections, primarily between area 44/45 and IPL areas. Connections between area 44 and hIP1 ($p = 0.002$), hIP3 ($p = 0.003$), PFcm ($p = 0.003$), PFm ($p = 0.002$), PFt ($p = 0.019$), and PGa ($p = 0.016$) were significant between hemispheres, while this was true for most area 45 couplings except for three (PFcm, $p = 0.105$; 5Ci, $p = 0.545$; 5M, $p = 0.190$). IFS couplings were comparatively variable among subjects, with most tracts being among clusters C and D, especially to parietal sulcal areas. On the contrary, area 44 and 45 connectivity was less variable, including cluster A and B couplings with all parietal ROIs but hIP1.

PMv provided the overall shortest path lengths to parietal areas, connecting strongly to many IPL and posterior SPL areas and, together with PM6d1, to the whole aIPS (significant for PMv-hIP1, $p = 0.003$; PMv-hIP3, $p \leq 0.001$; and PM6d1-hIP1, $p = 0.002$), with most couplings belonging to the least variable clusters A and B. For the PMC, PM6d3 links were the most variable, especially with IPS areas. Dorsal premotor and SMAs showed diverging linkage, compared with their inferior frontal counterparts, with strongest couplings to all anterior SPL nodes. PreSMA and, most notably, SMAproper were well associated with areas 7A ($p \leq 0.001$, $p = 0.006$) and 7PC ($p \leq 0.001$, $p = 0.007$), the former grouped in clusters A and B, denoting low variability among subjects.

From the perspective of the PPC, left aIPS mainly coupled with area 44/45, IFJ, and PMv, with hIP2 showing the least connectivity of the three subdomains. In the left IPL, PFm and PGa had especially strong connections with area 44/45 and PMv. In the left pIPS, hIP6 had the strongest connections to the frontal cortex, particularly again to area 44 and PMv, while the remaining ROIs poorly, and variably, connected to the frontal cortex. Finally, the left SPL areas showed a clear schism between anterior SPL, 7A and 7PC on the one hand and 7M plus 7P on the other, with the latter sparsely linking to frontal brain regions at all. 5Ci, 5L, and 5M highly linked to all of PMC and SMA; 7A had strong connections to PMv and SMAproper; and 7PC was linked with PM6d1, PMv, and both SMAs. Some of the most significant links ($p \leq 0.001$) of the SPL between hemispheres were area 45 (with 5L, 7A, 7PC, and 7P), IFS1–4 (with 7PC), PMv (with 7PC and 7P), and PreSMA (with 7PC and 7P). Most SPL links showed low variability between subjects.

Table 2. Distance matrix of left-sided fronto-parietal connectivity

	Area 44	Area 45	IFJ1	IFJ2	IFS1	IFS2	IFS3	IFS4	PM6d1	PM6d2	PM6d3	PMv	PreSMA	SMA
hiP1	11,6063	13,2595	13,9062	13,2249	14,6676	14,9842	14,7729	14,2688	12,9069	14,8215	14,7925	9,6432	16,2953	14,7424
hiP2	13,2518	14,905	15,5517	14,8704	16,3131	16,6297	16,4184	15,9135	14,5524	16,467	16,438	11,2887	17,9408	16,3879
hiP3	12,9609	14,6141	15,2608	14,5795	16,0222	16,3388	16,1275	15,6226	14,2615	16,1761	16,1471	10,9978	16,8727	15,007
PF	14,8508	16,504	17,1507	16,4694	17,9121	18,2287	18,0174	17,5125	16,1514	18,066	18,037	12,8877	19,5398	17,9869
PFcm	16,4877	18,1409	18,7876	18,1063	19,549	19,8656	19,6543	19,1494	17,7883	19,7029	19,6739	14,5246	21,1767	19,6238
PFm	13,8221	15,4753	16,122	15,4407	16,8834	17,2	16,9887	16,4838	15,1227	17,0373	17,0083	11,859	18,5111	16,9582
PFop	17,1488	18,802	19,4487	18,7674	20,2101	20,5267	20,3154	19,8105	18,4494	20,364	20,335	15,1857	21,8378	20,2849
PFt	15,5127	17,1659	17,8126	17,1313	18,574	18,8906	18,6793	18,1744	16,8133	18,7279	18,6989	13,5486	20,2017	18,6488
PGa	14,1482	15,8014	16,4481	15,7668	17,2095	17,5261	17,3148	16,8099	15,4488	17,3634	17,344	12,1851	18,8372	17,2843
PGp	16,0761	17,7293	18,376	17,6947	19,1374	19,454	19,2427	18,7378	17,3767	19,2913	19,2623	14,113	20,7651	19,2122
hiP4	18,3925	20,0457	20,6924	20,0111	21,4538	21,7704	21,5591	21,0542	19,6931	21,6077	21,5787	16,4294	22,767	20,9013
hiP5	17,4925	19,1457	19,7924	19,1111	20,5538	20,8704	20,6591	20,1542	18,7931	20,7077	20,6787	15,5294	20,6919	18,8262
hiP6	14,7023	16,3555	17,0022	16,3209	17,7636	18,0802	17,8689	17,364	16,0029	17,9175	17,8885	12,7392	17,9391	16,0734
hiP7	19,6688	21,322	21,9687	21,2874	22,7301	23,0467	22,8354	22,3305	20,9694	22,884	22,855	17,7057	21,4913	19,6256
hiP8	18,8151	20,4683	21,115	20,4337	21,8764	22,193	21,9817	21,4768	18,8965	20,4005	21,1133	16,852	18,9267	17,061
PO1	19,6877	21,3409	21,9876	21,3063	22,749	23,0656	22,8543	22,3494	19,7691	21,2731	21,9859	17,7246	19,7993	17,9336
5Ci	17,1222	18,7754	19,4221	18,7408	20,1835	20,5001	20,2888	19,7839	11,8954	13,3994	14,1122	15,1591	11,9256	10,0599
5L	16,6895	18,3427	18,9894	18,3081	19,7508	20,0674	19,8561	19,3512	12,7436	14,2476	14,9604	14,7264	12,7738	10,9081
5M	16,0551	17,7083	18,355	17,6737	19,1164	19,433	19,2217	18,7168	10,8283	12,3323	13,0451	14,092	10,8585	8,9928
7A	14,861	16,5142	17,1609	16,4796	17,9223	18,2389	18,0276	17,5227	14,9424	16,4464	17,1592	12,8979	14,9726	13,1069
7M	18,3627	20,0159	20,6626	19,9813	21,424	21,7406	21,5293	21,0244	18,4441	19,9481	20,6609	16,3996	18,4743	16,6086
7PC	14,8753	16,5285	17,1752	16,4939	17,9366	18,2532	18,0419	17,537	14,5578	16,0618	16,7746	12,9122	14,588	12,7223
7P	16,6583	18,3115	18,9582	18,2769	19,7196	20,0362	19,8249	19,32	16,7397	18,2437	18,9565	14,6952	16,7699	14,9042

Shortest weighted path matrix (D) by Dijkstra's algorithm. Normalized, undirected, parieto-premotor graph with highest density threshold (0.01) for the left hemisphere. Coloring indicates a value below a certain percentile in the network: Below 15th percentile (red), 25th percentile (dark orange), 50th percentile (light orange), and 75th percentile (yellow), respectively.

Table 3. Distance matrix of right-sided fronto-parietal connectivity

	Area 44	Area 45	IFJ1	IFJ2	IFS1	IFS2	IFS3	IFS4	PM6d1	PM6d2	PM6d3	PMv	PreSMA	SMA
hIP1	9,7415	10,9362	9,0297	8,0233	12,418	11,5958	11,3861	10,5492	8,1084	9,3502	7,8988	5,2056	10,8031	9,7987
hIP2	11,4532	12,6479	10,7414	9,735	14,1297	13,3075	13,0978	12,2609	9,8201	11,0619	9,6105	6,9173	12,5148	11,5104
hIP3	11,3914	12,5861	10,6796	9,6732	14,0679	13,2457	13,036	12,1991	9,7583	11,0001	9,5487	6,8555	12,453	11,4486
PF	13,5842	14,7789	12,8724	11,866	16,2607	15,4385	15,2288	14,3919	11,9511	13,1929	11,7415	9,0483	14,6458	13,6414
PFcm	14,958	16,1527	14,2462	13,2398	17,6345	16,8123	16,6026	15,7657	13,3249	14,5667	13,1153	10,4221	16,0196	15,0152
PFm	11,5215	12,7162	10,8097	9,8033	14,198	13,3758	13,1661	12,3292	9,8884	11,1302	9,6788	6,9856	12,5831	11,5787
PFop	15,6913	16,886	14,9795	13,9731	18,3678	17,5456	17,3359	16,499	14,0582	15,3	13,8486	11,1554	16,7529	15,7485
Pft	14,3152	15,5099	13,6034	12,597	16,9917	16,1695	15,9598	15,1229	12,6821	13,9239	12,4725	9,7793	15,3768	14,3724
PGa	11,9297	13,1244	11,2179	10,2115	14,6062	13,784	13,5743	12,7374	10,2966	11,5384	10,087	7,3938	12,9913	11,9869
PGp	13,9087	15,1034	13,1969	12,1905	16,5852	15,763	15,5533	14,7164	12,2756	13,5174	12,066	9,3728	14,9703	13,9659
hIP4	15,7891	16,9838	15,0773	14,0709	18,4656	17,6434	17,4337	16,5968	14,156	15,3978	13,9464	11,2532	16,8507	15,8463
hIP5	14,1141	15,3088	13,4023	12,3959	16,7906	15,9684	15,7587	14,9218	12,481	13,7228	12,2714	9,5782	15,1757	14,1713
hIP6	11,423	12,6177	10,7112	9,7048	14,0995	13,2773	13,0676	12,2307	9,7899	11,0317	9,5803	6,8871	12,4846	11,4802
hIP7	16,2132	17,4079	15,5014	14,495	18,8897	18,0675	17,8578	17,0209	14,5801	15,8219	14,3705	11,6773	17,2748	16,2704
hIP8	14,4709	15,6656	13,7591	12,7527	17,1474	16,3252	16,1155	15,2786	12,8378	14,0796	12,6282	9,935	15,5325	14,5281
PO1	16,7191	17,9138	16,0073	15,0009	19,3956	18,5734	18,3637	17,5268	15,086	16,3278	14,8764	12,1832	17,7807	16,7763
5Ci	18,4086	19,6033	17,6968	16,6904	21,0851	20,2629	20,0532	19,2163	16,7755	18,0173	16,5659	13,8727	18,5633	16,3176
5L	15,2441	16,4388	14,5323	13,5259	17,9206	17,0984	16,8887	16,0518	13,611	14,8528	13,4014	10,7082	16,3057	15,3013
5M	17,2655	18,4602	16,5537	15,5473	19,942	19,1198	18,9101	18,0732	15,6324	16,8742	15,4228	12,7296	17,4202	15,1745
7A	13,1935	14,3882	12,4817	11,4753	15,87	15,0478	14,8381	14,0012	11,5604	12,8022	11,3508	8,6576	14,2551	13,2507
7M	16,9399	18,1346	16,2281	15,2217	19,6164	18,7942	18,5845	17,7476	15,3068	16,5486	15,0972	12,404	18,0015	16,9971
7PC	13,1087	14,3034	12,3969	11,3905	15,7852	14,963	14,7533	13,9164	11,4756	12,7174	11,266	8,5728	14,1703	13,1659
7P	14,9463	16,141	14,2345	13,2281	17,6228	16,8006	16,5909	15,754	13,3132	14,555	13,1036	10,4104	16,0079	15,0035

Shortest weighted path matrix (D) by Dijkstra's algorithm. Normalized, undirected, parieto-premotor graph with highest density threshold (0.01) for the right hemisphere. Coloring indicates a value below a certain percentile in the network: below 15th percentile (red), 25th percentile (dark orange), 50th percentile (light orange), and 75th percentile (yellow), respectively. Note that all over shortest paths were tendentially shorter than on the left.

Right Hemisphere Connectivity

Area 44/45 were remarkably less connected to the parietal cortex on the right than on the left, while IFJ1 and IFJ2 seemed to mirror area 44's role in the left cortex by coupling intensely and significantly with aIPS (IFJ1-hIP1, $p \leq 0.001$; IFJ2-hIP1, $p = 0.047$; IFJ1-hIP2, $p = 0.020$; IFJ1-hIP3, $p = 0.001$), PFm (with IFJ1, $p \leq 0.001$), PGa (with IFJ1, $p \leq 0.001$ and IFJ2, $p = 0.032$), and hIP6 (with IFJ1, $p = 0.019$). Least variability was found for areas 44 and 45, while sulcal connections had most variability, even though less for AIPS-IFS connections than on the left.

Core premotor areas heavily connected to the parietal cortex, with dorsal premotor areas also reaching PFm, PGa, and hIP6. Links between PM6d1 and PGa ($p = 0.005$), PM6d1 and hIP6 ($p = 0.027$), as well as PM6d3 and PGa ($p = 0.009$) were significantly lateralized. Compared with the left, especially PM6d2 had a larger share of cluster A and B connections especially with the IPL. Interestingly, both SMAproper and PreSMA lacked stronger couplings to any SPL area, in contrast to the left hemisphere, rather coupling with aIPS (SMAproper-hIP2, $p = 0.027$) and IPL (e.g., PreSMA-PFcm, $p = 0.002$; PreSMA-PFt, $p = 0.002$), nearly all of which fell under clusters A and B for a low CV.

The right aIPS provided strong connections to nearly all frontal ROIs, with hIP2 and hIP3 performing almost identically. From the IPL, similar to the left hemisphere, strongest couplings existed to PFm and PGa. In the right pIPS, only hIP6 had thorough connections with frontal areas, however, even stronger than on the left, notably to IFJ (significant to IFJ1, $p = 0.019$, but high variability) and all PMC areas (significant to PM6d1, $p = 0.027$, and PMv, $p \leq 0.001$, cluster B and C variability). Only 5L strongly coupled with PMv and while 7M and 7P resembled the situation in the left cortex, 7A and 7PC switched connections from area 44 (on the left) to IFJ2 (significant for 7PC-area 44, $p = 0.005$). Notably, SPL connections to PMv were even stronger than on the left (insignificant only to 7M, $p = 0.253$, all but one in cluster A).

Bilateral Node Characterization

After calculating the connectivity between frontal and parietal brain areas to describe *where* information is primarily transferred, we were interested in analyzing, *which* of the network hubs is responsible for local or long-distance exchange. The idea behind this was that the connectional fingerprint of a brain area can define its structural role in a network (Passingham et al., 2002).

Therefore, brain areas were classified into nine categories of nodes in the network using a two-stage evaluation process: We first checked for hub criteria, using the PC and the WMDZ for each brain area. Second, we analyzed the integrative features of the hub by measuring its "strength" and NBC. Please find a more detailed explanation of the used GTA tools and their interpretation in the [Materials and Methods](#) section as well as a further discussion in the [Supporting Information \(Supplementary Discussion\)](#).

In short, there were two types of hubs, based on nomenclature from the literature (Passingham et al., 2002; Rubinov & Sporns, 2010; Sporns et al., 2007): connector hubs, which are nodes that are important for (global) intermodular integration (Rubinov & Sporns, 2010) and have a PC above the third quartile of the network, and provincial hubs, facilitating modular segregation and local connectivity (Rubinov & Sporns, 2010) that are above the third quartile of nodes in WMDZ graphs.

Table 4. Bilateral node character assignment

Left	Connector hub	Provincial hub
Rich central	hIP3, PGa, hIP6, 7A	Area 45, hIP1, hIP2, PF, 5L
Rich	–	hPO1, IFS3
Poor central	PMv, PGp, 7PC, 7P	–
Poor	–	PM6d2
Right	Connector hub	Provincial hub
Rich central	PMv, hIP1, hIP3, PGp, hIP6, 7A	IFS4, PFm
Rich	–	Area 45, hIP5, hIP8
Poor central	7PC	PM6d1, PM6d2, 5L, 5M
Poor	PGa	–

Nodes in the left and right hemisphere were assigned a network role considering their hub properties using a two-stage characterization approach. Connector or provincial hubs were further specialized as rich central, rich, poor central, and poor, respectively.

These hubs were further assigned one of four categories to differentiate their exact role in the networks. We called a hub “rich” if the node strength (or “degree”) was among the top 50% of all nodes, “rich central” if NBC was additionally among the top 50% of nodes, “poor central” if only NBC was above the 50th percentile of all nodes, and “poor” if strength as well as NBC values lay below the 50th percentile. Central hubs lie on shortest paths (i.e., strong connections) between brain areas within (provincial hubs) or between modules (connector hubs) of a network. Please find a schematic visualization of hub roles in the network as Supporting Information Figure S3. The detailed hub assignment is given in Table 4.

All nodes that did not match PC and WMDZ criteria, called “nonhubs,” could be further specified as peripheral nodes, if both NDC and strength values were among the lowest (i.e., below the first quartile) in the networks (Zhang et al., 2021). We identified left PM6d3, right PreSMA, SMAproper, and PFcm as well as bilateral PFop, 5Ci, and 7M as peripheral nodes for having both strength and NBC values below the 25th percentile.

DISCUSSION

In the current study, we used multishell DW-MRI, tractography, and GTA techniques to investigate the structural connectivity between concisely parcellated parietal and premotor brain areas in the human cortex. We did find not only distinct patterns of parieto-premotor pathway segments but also clear signs of lateralization between hemispheres.

A Third, Lateralized Dorsal Substream?

Visuomotor transformation for tool use is known to be processed along two different, interconnected parts of the parieto-frontal dorsal stream: the dorso-dorsal and the ventro-dorsal pathway (Binkofski & Buxbaum, 2013; Rizzolatti & Matelli, 2003). In the present depiction of the dorsal stream, intra- and interhemispheric gradation of connectivity becomes evident. Parieto-frontal information might be processed in more than two dorsal substreams, differing in the two hemispheres. Please find a visual delineation in Figures 3.1 and 3.2. The BrainNet Viewer

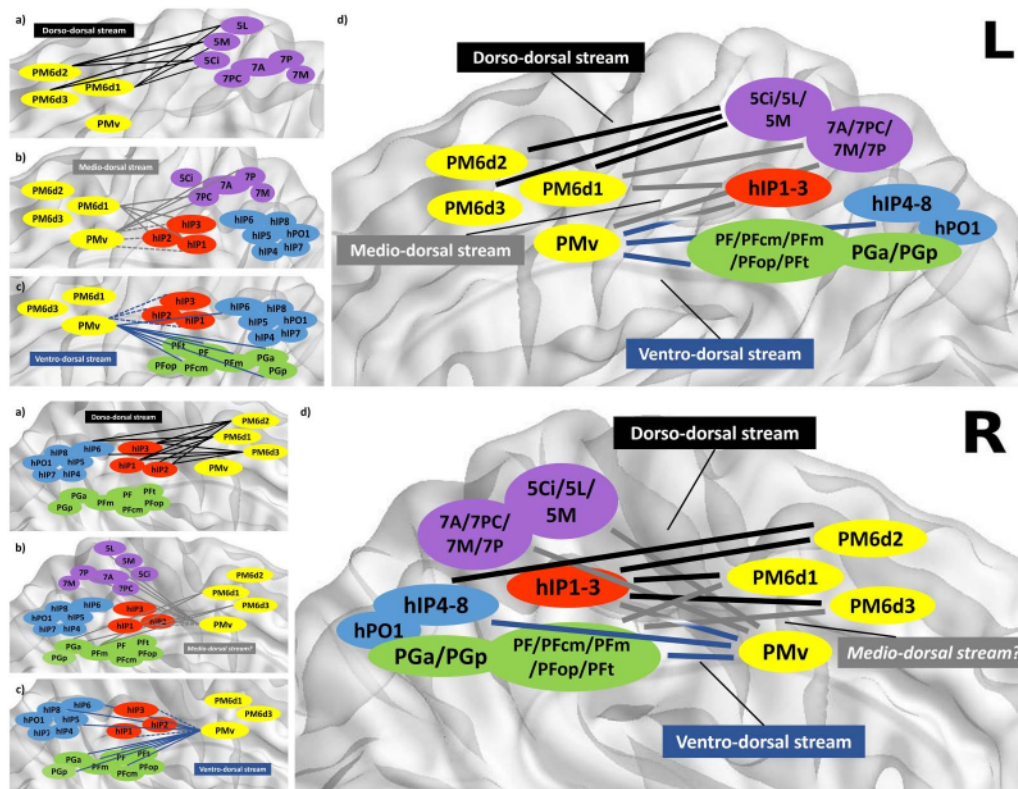


Figure 3. Outline of a lateralized dorsal stream, left hemisphere. 3.1. Depiction of strongest links (below the 15th percentile in the undirected distance matrix) between frontal and parietal ROIs in the left (L) hemisphere. (A–C) Detailed couplings of three overlapping substreams of the dorsal stream, comprising a dorso-dorsal (black), medio-dorsal (gray), and ventro-dorsal (blue) pathway. A schematic overview is given in (D). The two-colored (D) and dotted (B, C) hIP1–3/PMv arrows indicate ambiguous affiliation of the stream. Outline of a lateralized dorsal stream, right hemisphere. 3.2. Depiction of strongest links (below the 15th percentile in the undirected distance matrix) between frontal and parietal ROIs in the right (R) hemisphere. (A–C) Detailed connectivity in three overlapping substreams of the dorsal stream. A schematic overview is given in (D). A dorso-dorsal (black), medio-dorsal (gray), and ventro-dorsal (blue) pathway can be differentiated, putatively organized in a two- or threefold model, since a medio-dorsal pathway is less clearly delimitable than on the left. The two-colored (D) and dotted (B, C) hIP1–3/PMv arrows indicate ambiguous affiliation of the stream.

software (Version 1.7, URL: <https://www.nitrc.org/projects/bnv/>) was used for visualization (Xia et al., 2013).

On the left, gradation and segregation appear very clearly, in that anterior SPL connectivity becomes gradually weaker from dorsal to ventral, while posterior SPL, pIPS, and IPL couplings behave the other way around. This was similarly seen in earlier functional connectivity studies, where superior dorsal PMC was primarily connected to the dorsal parietal domains and inferior PMd coupled strongly with intraparietal sulcal areas, while inferior parietal areas were well connected with the ventral PMC, presumably for grasping and tool use (Mars et al., 2011). Area aIPS performs in a slightly intermediate fashion, following an increasing dorso-ventral gradient as well, but without disconnecting from PMd in the case of hIP1. This coincides with hIP1's role as a fronto-parietal connector hub and first hierarchy domain for goal-directed movements (Verhagen et al., 2013). Intriguingly, dorso-ventral gradation in the parietal cortex does not split patterns into a PMd and PMv pathway, but rather shows similar connectivity patterns of PMd1 and PMv, drawing a fluent passage through the three dorsal premotor ROIs. This might be due to the more rostro-ventral position of PMd1, but

differences in the opposite hemisphere makes this purely topographical explanation questionable. Instead, we assume that the not-yet-subparcellated area PMv is further subdividable as well, putatively between a more ventral (“ventro-dorsal”) and a more dorsal (“medio-dorsal”) portion, the latter converging with PM6d1 in connective patterns. A threefold division of the parieto-frontal dorsal stream therefore propagates left-sided sensorimotor information on individual, but cross-linked processing pathways. Such interstream links were recently described for macaques (Greulich et al., 2020).

In our model, the dorso-dorsal path connects dorsal SPL with rostro-dorsal PMd, significant for 5Ci ($p = 0.002$, $p = 0.016$), 7M ($p = 0.023$, $p = 0.007$), and 7PC ($p = 0.001$, $p = 0.014$) to both PM6d2 and PM6d3, putatively for reaching (Diedrichsen et al., 2005; Rizzolatti & Matelli, 2003), hand movements (Caspers et al., 2010), and visuospatial imagery (Genon et al., 2017). These functions are also confirmed by the fact that lesions to the dorso-dorsal stream are known to cause optic ataxia (Karnath & Perenin, 2005). A medio-dorsal section couples ventral SPL and parts of the IPS with intermediate PMd/v, associated in the literature with movement coordination in space (Tomassini et al., 2007) and manual object manipulation (Binkofski, Buccino, Stephan, et al., 1999). Ventro-dorsal fibers would process grasping (Tomassini et al., 2007), target-oriented action (Sakreida et al., 2016), and decision-making skills (Caspers et al., 2008) via IPL, aIPS, pIPS, and ventral PMv. IPL-PMv couplings, especially, might transfer important semantic information for environment interaction, since lesion studies have shown that both PGa/PGp as well as PMv are important for reading, writing, and speech error perception (Binkofski et al., 2016; Nuttall et al., 2018), and ventro-dorsal stream pathology includes limb apraxia (Pisella et al., 2006).

On the right, two main differences become apparent. Firstly, the gradation of sulcal areas is less pronounced, especially for aIPS and hIP6, which show little preference between ventral and dorsal premotor areas. Differences between left and right were significant for PM6d1-hIP1 ($p = 0.002$), PM6d1-hIP6 ($p = 0.027$), and PMv to hIP1 ($p = 0.003$), hIP3 ($p \leq 0.001$), and hIP6 ($p \leq 0.001$). Additionally, SPL-dorsal premotor connectivity is much weaker, posing the question whether dorso-dorsal information propagates beyond the current network (e.g., to the dorso-lateral prefrontal cortex [dlPFC], for which there is good evidence; Caspers et al., 2012; Greulich et al., 2020; Jung et al., 2018; Uddin et al., 2010) or becomes part of a “medio-dorsal” PMv stream, corresponding to a presumably different internal PMv division.

This becomes more likely since, secondly, clear differences between connectivity fingerprints of dorsal premotor areas are absent in the right hemisphere, appearing much more as a unity than on the left, with PM6d1 and PM6d3 performing almost identically. A connective “boundary” appears more probable between right PMd and PMv, with the assumption of an internal splitting of upper and lower PMv. This is in accordance with not only more sulcal and inferior parietal links of right PMd, mostly significant for PM6d1 (e.g., PM6d1-hIP1, $p = 0.002$), but also for links between IPL and PM6d2 (e.g., with PFcm, $p = 0.003$) and PM6d3 (with PGa, $p = 0.009$), while PMv connectivity keeps mainly the same. As a consequence, visuomotor transformation on the right is either propagated via three slightly different streams (even though also of a ventral, medial, and dorsal design) or through the previously established dyad, fitting the model of a ventral and dorsal attentional system (Corbetta & Shulman, 2011), for instance. It is also important to note that a differentiation into substreams might occur earlier or later in their courses, similarly seen very recently for the human visual pathway between temporal and IPL areas (Choi et al., 2020).

As a limitation, one must mention that PM6d2 and PM6d3 links to parietal sulcal areas were mostly nonsignificant between hemispheres (see Table 1), together with a medium to

high variability across subjects in PM6d3. This shows the need for verification of the current gyro-sulcal connections in a larger cohort.

This also casts new light on the well-established anatomical concept of three distinct superior longitudinal fasciculi (SLFs) (Thiebaut de Schotten, Dell'Acqua, et al., 2011). Dorsal SLF1, associated with voluntary orienting of spatial attention toward visual targets (Corbetta & Shulman, 2002), matches with parts of the left dorso-dorsal and SMA networks (see below) in the current study. However, its right counterpart appears to be part of a more ventral “medio-dorsal” stream. One explanation for its “reduced” dorso-dorsal connectivity on the right in our study could be that it is overlapping with the so-called dorsal visuospatial pathway, connecting occipitoparietal cortex and IPL with the dlPFC (Uddin et al., 2010), with the latter not being part of our current network and therefore missing in fiber track counts.

The middle SLF2 is thought to communicate between its dorsal and ventral neighbors as a modulator for dorsal networks (Thiebaut de Schotten, Dell'Acqua, et al., 2011), which can be compared with especially strong aIPS connectivity on the right and fits to our medio-dorsal substream on the left. Thiebaut de Schotten and colleagues described it as rather right-lateralized (Thiebaut de Schotten, Dell'Acqua, et al., 2011) so we assume that it is currently mirrored by stressed ventro-dorsal long-distance couplings, as between SPL and PMv, putatively forming a distinct medio-dorsal pathway on the right.

The ventral-most SLF3 is thought to get activated through automatic capture of spatial attention by visual targets (Corbetta & Shulman, 2002), probably overlapping with the arcuate fasciculus (AF) (Thiebaut de Schotten, Ffytche, et al., 2011). It is currently mirrored by IPS/IPL-PMv patterns in both hemispheres, seemingly the most stable in the network. Since PMv connectivity is complemented by even stronger SPL input on the right, such previously proposed lateralization (Thiebaut de Schotten, Dell'Acqua, et al., 2011) is confirmed by our data. However, its prefrontal aspects might be further accentuated by the “Broca's-IFJ switch” (see below), with right-sided information predominantly reaching IFS areas, presumably for attention processing.

A Functional Dichotomy of the SMA

The SMA is a highly sophisticated motor region of the human cortex that deals with motor learning, action sequencing, and rhythmicity (Genon et al., 2017).

The left-sided SPL connectivity of the SMA confirms its role in converting sensory input through gyro-gyral dorsal parietal pathways, forming a putative part of the dorso-dorsal stream. This would encompass areas 7PC and 7P, which were designated as poor-central connector hubs, therefore forming important domains for integration of the SPL.

Similar to right-sided SPL areas 5Ci, 5L, and 5M, the SMAs of the right hemisphere lack most of their dorsal parieto-frontal connections, significant especially for PreSMA (with 5Ci, $p = 0.001$ and 5M, $p = 0.006$). It is highly probable that such hemispheric divergence reflects functional segregation for multitask processing and might serve as an equivalent of proposed long-reach association fibers of the SPL (Caspers et al., 2012). Dorso-ventrally graded, right-sided gyro-sulcal and gyro-gyral couplings of the SMA with aIPS and IPL might, for instance, enable listening abilities, including attentional and executive processes (Hesling et al., 2019). A very interesting case of a patient with isolated gait apraxia after localized bilateral SMA infarction due to an anterior cerebral artery anomaly might underpin functionally relevant ventral parietal information flow to the right SMA (Della Sala et al., 2002). Especially, IPL shows

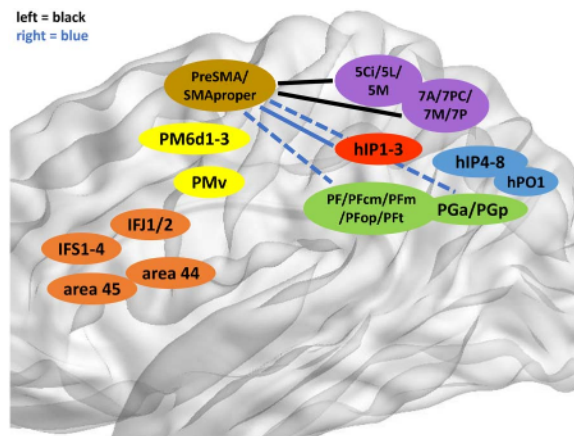


Figure 4. Outline of the SMA dichotomy. Depiction of strongest links between SMA and parietal ROIs on the left (black) and right (blue). For reasons of comparison, the left and right connectivities are both projected on the brain's left hemisphere. A left dorso-dorsal pattern clearly differs from a right ventro-dorsal pattern. Continuous arrows indicate strongest connectivity (below the 15th percentile) in the undirected distance matrix, while dotted arrows stand for connectivity below the first quartile but above the 15th percentile.

strong connectivity with SMAproper in the right hemisphere (although insignificant, see Table 1), inspiring the idea that reciprocal SMA-IPL circuits could serve a more cognitive role in action understanding (Hertrich et al., 2016) and coordination of varying sensorimotor modalities (Nachev et al., 2008). On the other hand, considerably fewer parietal connections of the right SMA could reflect its putative right-lateralized integration into a cortico-subcortico-cerebellar motor network (Genon et al., 2017). A schematic overview of this SMA dichotomy can be examined in Figure 4.

As a sidenote, the fact that 7M had no strong frontal couplings whatsoever is presumably congruent with its role as a “connective bridge” to the temporal, rather than frontal lobe (Jung et al., 2017), similar to the occipito-parietal hub position of PGp (Caspers et al., 2013).

The Broca's-IFJ Switch

In the current data, connectivity between ventrolateral prefrontal and inferior parietal areas is substantially lateralized and segregated between two frontal domains. On the left, area 44 shows predominant gyro-sulcal and gyro-gyral connections with aIPS, hIP6, and IPL (especially PGa and PFm), for the most part significant (e.g., area 44-hIP1, $p = 0.002$), most probably involved in language processing (Binkofski et al., 2016; Caspers et al., 2011, 2013; Richter et al., 2019), hand movements, and object interaction (Binkofski, Buccino, Posse, et al., 1999). Right-sided IFS areas (especially IFJ) mirror this pattern (significant, e.g., IFJ1-hIP1, $p \leq 0.001$), connoting a right-dominant intersulcal information flow between the IFS and the IPS, putatively serving attentional tasks (Caspers et al., 2011, 2012; Corbetta & Shulman, 2002) and working memory (Richter et al., 2019; Van Doren et al., 2010), which could therefore spread parallelly, enabling distinct multitask abilities. We call this a lateralized “Broca's-IFJ switch” between motor-language (left) and attentional faculties (right).

When compared visually, the most striking difference between hemispheres are twofold streams connecting the aIPS and area 44/45 on the left, which represent the direct long segment and the indirect anterior segment (\approx SLF3) of the AF, with only the former substantially

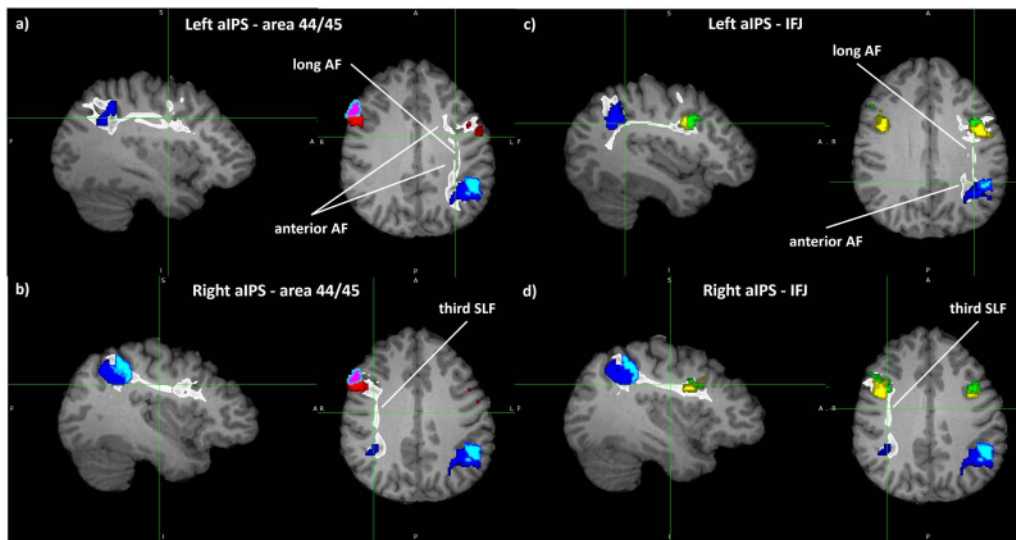


Figure 5. Depiction of bilateral tracts between aIPS, area 44/45, and IFJ. Exemplary single-subject visualization of connecting fiber tracts between the anterior intraparietal sulcus (aIPS) and area 44/45 (A, B) as well as the inferior frontal junction (IFJ) (C, D) in sagittal (left subimage) and axial (right subimage) planes. (A) The left-sided long (direct) and anterior segments of the AF connecting the aIPS and area 44/45 on the left. (B) The connecting third (ventral) part of the SLF between right-sided aIPS and area 55/45. (C) The left hemisphere course of both segments of the AF, with the long AF primarily connecting hIP1 and hIP2 with IFJ. The anterior AF does not substantially reach the IFJ but runs more dorso-medially. (D) Connections between the aIPS and IFJ via the third SLF in the right hemisphere. While two separate yet partially intertwined pathways form the connective routes on the left, a more uniform right sided pathway can be differentiated. Tracts (white) were generated probabilistically and bidirectionally, a brightness threshold between 10,000 and 15,000 as well as linear interpolation were used for illustration purposes in fsleyes (DOI: 10.5281/zenodo.7038115). Note that the software uses radiological space for template depiction, so left and right orientation is switched. The thin light green cross marks the position of focus in all three planes. Areas included: hIP1 (dark blue), hIP2 (light blue), area 44 (red), and area 45 (purple). A = anterior, P = posterior, L = left, R = right.

carrying fibers to IFJ. This is in accordance with the fact that the AF was shown to be left lateralized and therefore presumably more clearly presents its two main fronto-parietal branches in the left hemisphere (Thiebaut de Schotten, Ffytche, et al., 2011). On the right, aIPS-VLPFC routes seem to propagate more coherently in what resembles the third SLF. The hemispheric difference in connectivity could therefore also be mirrored in the difference of larger pathway architecture. A depiction of this can be found in Figures 5.1 and 5.2.

For both patterns, we find a dorsal to ventral gradation in connectivity strength. Notably, the “weaker” pattern of each hemisphere still solidly couples with most of aIPS, fittingly designated as rich-central connector hubs (left hIP3, right hIP1, and hIP3), along with hIP6 and PGa. Therefore, the “weaker” network part of each side would complement the main hemispheric function, that is, right-sided area 44 is involved in movement attention in space (Binkofski et al., 2000) and left-sided IFS areas are also activated by words and pictures (Van Doren et al., 2010). The right rich-central provincial hub PFM is in accordance with its proposed function as a (local) transition spot between the supramarginal and the angular gyrus (Binkofski et al., 2016).

Lastly, the functional relevance of the switch is obvious in that right-sided disruption of fibers connecting parietal and prefrontal areas lead to visuospatial neglect (Urbanski et al., 2008), while congruent left-sided lesions can cause aphasia (Madhavan et al., 2016) and apraxia (Culham & Valyear, 2006).

Gyral and Sulcal Connectivity

It became evident that gyri and sulci have different connectivity properties and, therefore, functional roles in cortical networks (Jiang et al., 2018). While gyri mostly serve as interregional connection centers, sulci often represent local integration units (Deng et al., 2014).

Gyro-gyral connections were stated to represent the strongest functional pathways, transmitting information among remote brain regions. This could be confirmed by long-distance couplings between larger gyral ROIs in the premotor (e.g., PMv and area 44) and PPC (e.g., PFm, PGa, and 5M). Size and position can substantially influence (and possibly overestimate) the functional role assigned to an ROI in a network, which is discussed in more detail in the *Methodical Limitations* section.

Gyro-sulcal couplings are thought to have “moderate” functionality as links between intra- and interregional routes. This is especially interesting for aIPS areas, having a topographically exposed position close to the central sulcus, representing an intersection point for both core premotor and (right-sided) supplementary motor areas as well as areas 44 and 45 on the left. Hence, we would like to stimulate the idea that sulcal areas in strategic positions, like hIP1, for instance, can be of higher functional relevance for pathway integration as formerly thought. Intersulcal connections are known for forming indirect circuits via gyri for long-distance integration (Deng et al., 2014), often assigned a purely local network aspect. In the current study, links between aIPS and pIPS, hIP1 and hIP6 in particular, with IFS areas prove that long-distance intersulcal connections complement gyral information flow. These could form putative simultaneous processing pathways for parallel information flow in the cortex, seen for the “Broca’s-IFJ switch,” possibly as grouped clusters of smaller brain areas forming local (and probably also regional) network hubs.

Methodical Limitations

Importantly, the current study has focused on a distinct set of brain areas, covering portions of association cortices in the frontal and parietal lobe involved in motor activity, tool use, space perception, and interaction. With the advantage of a more concise investigation of intranetwork connectivity comes the disadvantage of excluding several neighboring brain regions, especially in the frontal cortex, potentially incorporated in some of the depicted subnetworks. It is therefore reasonable to put the presented results into relation with future connectivity studies, exploring associated structural and functional cortical networks.

It is important to mention that advanced multishell Diffusion Weighted Imaging and tractography implicate methodical limitations. Most notably, it remains difficult to reconstruct intersecting, crossing, or bordering streamlines, whereas smallest white matter fibers are generally not identifiable at all (Tournier et al., 2011).

Biases of tractography usually include the following (Girard et al., 2020): (a) Algorithms tend to better reconstruct short, large, and straight pathways; (b) streamlines close to gray matter or cerebrospinal fluid voxels tend to be underrepresented, sometimes causing spurious or incomplete fibers; and (c) pathways on the gyral crown are preferably considered in outputs as opposed to those in gyral walls. The latter aspect appears especially crucial since we aimed at depicting concise connectivity patterns as well in gyri as in sulci, even between small brain areas. Apart from possible anatomical reasons, the technical causes for this bias comprise voxel size, a low curvature threshold, and whole-brain seeding (Schilling et al., 2018). To compensate for this, we used a high-resolution voxel design, refrained from whole-brain seeding and aimed at explicitly depicting smaller connections by subdividing the network and

averaging results. Another example for this gyral bias is inherent to the approach of using the CV, which is especially sensitive to changes in smaller mean values close to 0 and is therefore less meaningful for connection strength values of sulcal ROIs, typically yielding smaller streamline counts.

Conversely, small ROIs can affect the reconstruction of network pathways, being irregularly shaped or having a prominent position on a gyrus, influencing the depicted course of a pathway. We tried to compensate for this circumstance by using groups of smaller ROIs rather than single ROIs to assign segments of pathways and by drawing on centroid positions of ROIs in pathway visualization.

Although inverting streamline weights to lengths is deemed a suitable measure for interpretation of connectivity strengths (Yeh et al., 2021), it is important to mention that short distances can occur due to topographic proximity, high-edge weights as well as many edges connecting two nodes. Thereby, length values can have differing reasons, not always identical with what we understand as a “linkage” in the sense of internodal communication.

Another limitation specific to the present study is the use of a manually created ROI PMv, which was defined in collaboration with a neuroanatomist Svenja Caspers (SC) based on its established cortical position. On the one hand, it remains more difficult to compare with the rest of ROIs since it was not commensurably defined in its shape and subparcellation. On the other hand, due to its relatively large volume, it tends to “absorb” streamlines from parietal seeds, having strong impact on cutoff selection and centrality measures. Therefore, a reevaluation of the current PMv connectivity is recommendable with the use of multimodal parcellation.

Conclusions

The current study had three major results concerning structural connectivity between human parietal and premotor brain areas:

1. A triadic dorsal stream,
2. heavily lateralized SMA couplings, and
3. a “switch” in connectivity patterns of area 44/45 and the IFJ between hemispheres.

Although less prominent on the right, a gradient of interconnected, yet distinct, substreams for visual perception and object manipulation serves as the anatomical equivalent of a functional gradient that both the dorsal stream and the ventral stream represent. We know that the visual guidance of action is mainly processed via the dorsal stream (originally starting in the primary visual cortex), while the semantic and cognitive aspects are largely processed ventrally (Goodale & Milner, 1992). Aside from the already deciphered dorso-dorsal and ventro-dorsal substreams, a medio-dorsal pathway, emerging in the parietal cortex and connecting mainly SPL, aIPS, PMv, and PM6d1 (again, depending on the hemisphere), is mainly gyro-sulcal and could be involved in hand motor function and direct object manipulation (Binkofski, Buccino, Stephan, et al., 1999; Jeannerod et al., 1995). With new insights into the internal subdivision of the ventral PMC, we will hopefully learn more about the exact anatomic groundwork of this processing path.

The found that the “dichotomy” of supplementary motor connectivity with the PPC builds upon knowledge on hemisphere-specific motor processing. Dorsally oriented couplings on the left would be closely related to the neighboring dorso-dorsal stream fibers, transferring sensory information about animate objects in space. Its right counterpart would rather serve attentional and cognitive functions in object interaction, necessary for multitask movement processing.

Similarly, ventrolateral prefrontal connections of the aIPS primarily reach areas 44 and 45 on the left for linguistic aspects of motor activity, whereas right-sided couplings are largely intersulcal, communicating attentional information via the IFS. This finding is especially relevant for understanding human cortex functioning as a bilateral, simultaneous network system, considering that structural and functional lateralization is scarcely developed in nonhuman primates.

ACKNOWLEDGMENTS

We are grateful to H. Chen for her significant contribution to the implementation of pre- and postprocessing pipelines as well as MRI scanning; K. Willmes for his helpful advice on statistical measures; A. Schüppen and O. Poznansky for their notable inputs on DW-MRI processing techniques; J. Schreiber for his contribution to the ROI registration algorithm; A. Pellicano and H. Patel for their vital input regarding conceptualization. All figures in this study were conceptualized and illustrated by M.J.

SUPPORTING INFORMATION

Supporting information for this article is available at https://doi.org/10.1162/netn_a_00407.

AUTHOR CONTRIBUTIONS

Marvin Jüchtern: Data curation; Formal analysis; Investigation; Methodology; Software; Validation; Visualization; Writing – original draft; Writing – review & editing. Usman Jawed Shaikh: Formal analysis; Investigation; Methodology; Software; Validation. Svenja Caspers: Conceptualization; Formal analysis; Funding acquisition; Methodology; Project administration; Supervision; Writing – review & editing. Ferdinand Binkofski: Conceptualization; Formal analysis; Investigation; Methodology; Project administration; Resources; Supervision; Writing – review & editing.

FUNDING INFORMATION

Svenja Caspers, Horizon 2020 Framework Programme (<https://doi.org/10.3030/945539>), Award ID: Grant Agreement No. 945539; HBP SGA3.

DATA AVAILABILITY STATEMENT

The datasets generated and analyzed during the current study were newly acquired. All codes for pre- and postprocessing of this data were obtained from the software cited in the respective paragraph of the *Materials and Methods* section. Due to data privacy regulations of the study protocol by the ethics commission and national policy, raw data beyond the shared are available from the corresponding author on reasonable request with the need for a formal data sharing agreement. Anonymized raw connectivity matrices, aggregated whole-group bilateral thresholded connectivity, distance, node betweenness matrices, edge betweenness, and strength data are available via an open repository.

REFERENCES

- Amunts, K., Mohlberg, H., Bludau, S., & Zilles, K. (2020). Julich-Brain: A 3D probabilistic atlas of the human brain's cytoarchitecture. *Science*, 369(6506), 988–992. <https://doi.org/10.1126/science.abb4588>, PubMed: 32732281
- Andersson, J. L. R., Skare, S., & Ashburner, J. (2003). How to correct susceptibility distortions in spin-echo echo-planar images: Application to diffusion tensor imaging. *NeuroImage*, 20(2), 870–888. [https://doi.org/10.1016/S1053-8119\(03\)00336-7](https://doi.org/10.1016/S1053-8119(03)00336-7), PubMed: 14568458

- Andersson, J. L. R., & Sotiropoulos, S. N. (2016). An integrated approach to correction for off-resonance effects and subject movement in diffusion MR imaging. *NeuroImage*, 125, 1063–1078. <https://doi.org/10.1016/j.neuroimage.2015.10.019>, PubMed: 26481672
- Behrens, T. E. J., Berg, H. J., Jbabdi, S., Rushworth, M. F. S., & Woolrich, M. W. (2007). Probabilistic diffusion tractography with multiple fibre orientations: What can we gain? *NeuroImage*, 34(1), 144–155. <https://doi.org/10.1016/j.neuroimage.2006.09.018>, PubMed: 17070705
- Benjamini, Y., & Hochberg, Y. (1995). Controlling the false discovery rate: A practical and powerful approach to multiple testing. *Journal of the Royal Statistical Society: Series B (Methodological)*, 57(1), 289–300. <https://doi.org/10.1111/j.2517-6161.1995.tb02031.x>
- Binkofski, F., Amunts, K., Stephan, K. M., Posse, S., Schormann, T., Freund, H. J., ... Seitz, R. J. (2000). Broca's region subserves imagery of motion: A combined cytoarchitectonic and fMRI study. *Human Brain Mapping*, 11(4), 273–285. [https://doi.org/10.1002/1097-0193\(200012\)11:4<273::AID-HBM40>3.0.CO;2-0](https://doi.org/10.1002/1097-0193(200012)11:4<273::AID-HBM40>3.0.CO;2-0), PubMed: 11144756
- Binkofski, F., Buccino, G., Posse, S., Seitz, R. J., Rizzolatti, G., & Freund, H. (1999). A fronto-parietal circuit for object manipulation in man: Evidence from an fMRI-study. *European Journal of Neuroscience*, 11(9), 3276–3286. <https://doi.org/10.1046/j.1460-9568.1999.00753.x>, PubMed: 10510191
- Binkofski, F., Buccino, G., Stephan, K. M., Rizzolatti, G., Seitz, R. J., & Freund, H. J. (1999). A parieto-premotor network for object manipulation: Evidence from neuroimaging. *Experimental Brain Research*, 128(1–2), 210–213. <https://doi.org/10.1007/s002210050838>, PubMed: 10473761
- Binkofski, F., & Buxbaum, L. J. (2013). Two action systems in the human brain. *Brain and Language*, 127(2), 222–229. <https://doi.org/10.1016/j.bandl.2012.07.007>, PubMed: 22889467
- Binkofski, F. C., Klann, J., & Caspers, S. (2016). On the neuroanatomy and functional role of the inferior parietal lobule and intra-parietal sulcus In G. Hickok & S. L. Small (Eds.), *Neurobiology of language* (pp. 35–47). Elsevier. <https://doi.org/10.1016/B978-0-12-407794-2.00004-3>
- Bradler, S. H. (2015). *Multimodal mapping and function of the inferior frontal sulcus of the human brain* (Doctoral dissertation, Heinrich-Heine-Universität Düsseldorf). Retrieved from <https://docserv.uni-duesseldorf.de/servlets/DocumentServlet?id=33152>.
- Brandes, U. (2001). A faster algorithm for betweenness centrality. *Journal of Mathematical Sociology*, 25(2), 163–177. <https://doi.org/10.1080/0022250X.2001.9990249>
- Brozzoli, C., Gentile, G., Petkova, V. I., & Ehrsson, H. H. (2011). FMRI adaptation reveals a cortical mechanism for the coding of space near the hand. *Journal of Neuroscience*, 31(24), 9023–9031. <https://doi.org/10.1523/JNEUROSCI.1172-11.2011>, PubMed: 21677185
- Callan, D., Callan, A., Gamez, M., Sato, M. A., & Kawato, M. (2010). Premotor cortex mediates perceptual performance. *NeuroImage*, 51(2), 844–858. <https://doi.org/10.1016/j.neuroimage.2010.02.027>, PubMed: 20184959
- Cao, Q., Shu, N., An, L., Wang, P., Sun, L., Xia, M.-R., ... He, Y. (2013). Probabilistic diffusion tractography and graph theory analysis reveal abnormal white matter structural connectivity networks in drug-naïve boys with attention deficit/hyperactivity disorder. *Journal of Neuroscience*, 33(26), 10676–10687. <https://doi.org/10.1523/JNEUROSCI.4793-12.2013>, PubMed: 23804091
- Caspers, S., Amunts, K., & Zilles, K. (2012). Posterior parietal cortex: Multimodal association cortex. In J. K. Mai & G. Paxinos (Eds.), *The human nervous system* (pp. 1036–1055). Academic Press. <https://doi.org/10.1016/B978-0-12-374236-0.10028-8>
- Caspers, S., Eickhoff, S. B., Geyer, S., Scheperjans, F., Mohlberg, H., Zilles, K., & Amunts, K. (2008). The human inferior parietal lobule in stereotaxic space. *Brain Structure & Function*, 212(6), 481–495. <https://doi.org/10.1007/s00429-008-0195-z>, PubMed: 18651173
- Caspers, S., Eickhoff, S. B., Rick, T., von Kapri, A., Kühlen, T., Huang, R., ... Zilles, K. (2011). Probabilistic fibre tract analysis of cytoarchitectonically defined human inferior parietal lobule areas reveals similarities to macaques. *NeuroImage*, 58(2), 362–380. <https://doi.org/10.1016/j.neuroimage.2011.06.027>, PubMed: 21718787
- Caspers, S., Schleicher, A., Bacha-Trams, M., Palomero-Gallagher, N., Amunts, K., & Zilles, K. (2013). Organization of the human inferior parietal lobule based on receptor architectonics. *Cerebral Cortex*, 23(3), 615–628. <https://doi.org/10.1093/cercor/bhs048>, PubMed: 22375016
- Caspers, S., Zilles, K., Laird, A. R., & Eickhoff, S. B. (2010). ALE meta-analysis of action observation and imitation in the human brain. *NeuroImage*, 50(3), 1148–1167. <https://doi.org/10.1016/j.neuroimage.2009.12.112>, PubMed: 20056149
- Choi, S. H., Jeong, G., Kim, Y. B., & Cho, Z. H. (2020). Proposal for human visual pathway in the extrastriate cortex by fiber tracking method using diffusion-weighted MRI. *NeuroImage*, 220, 117145. <https://doi.org/10.1016/j.neuroimage.2020.117145>, PubMed: 32650055
- Cohen, J. R., & D'Esposito, M. (2016). The segregation and integration of distinct brain networks and their relationship to cognition. *Journal of Neuroscience*, 36(48), 12083–12094. <https://doi.org/10.1523/JNEUROSCI.2965-15.2016>, PubMed: 27903719
- Corbetta, M., & Shulman, G. L. (2002). Control of goal-directed and stimulus-driven attention in the brain. *Nature Reviews Neuroscience*, 3(3), 201–215. <https://doi.org/10.1038/nrn755>, PubMed: 11994752
- Corbetta, M., & Shulman, G. L. (2011). Spatial neglect and attention networks. *Annual Review of Neuroscience*, 34, 569–599. <https://doi.org/10.1146/annurev-neuro-061010-113731>, PubMed: 21692662
- Culham, J. C., & Valyear, K. F. (2006). Human parietal cortex in action. *Current Opinion in Neurobiology*, 16(2), 205–212. <https://doi.org/10.1016/j.conb.2006.03.005>, PubMed: 16563735
- Della Sala, S., Francescani, A., & Spinnler, H. (2002). Gait apraxia after bilateral supplementary motor area lesion. *Journal of Neurology, Neurosurgery, and Psychiatry*, 72(1), 77–85. <https://doi.org/10.1136/jnnp.72.1.77>, PubMed: 11784830
- Deng, F., Jiang, X., Zhu, D., Zhang, T., Li, K., Guo, L., & Liu, T. (2014). A functional model of cortical gyri and sulci. *Brain Structure & Function*, 219(4), 1473–1491. <https://doi.org/10.1007/s00429-013-0581-z>, PubMed: 23689502
- Diedrichsen, J., Hashambhoy, Y., Rane, T., & Shadmehr, R. (2005). Neural correlates of reach errors. *Journal of Neuroscience*, 25(43), 9919–9931. <https://doi.org/10.1523/JNEUROSCI.1874-05.2005>, PubMed: 16251440

- Dijkstra, E. W. (1959). A note on two problems in connexion with graphs. *Numerische Mathematik*, 1, 269–271. <https://doi.org/10.1007/BF01386390>
- Eickhoff, S. B., Stephan, K. E., Mohlberg, H., Grefkes, C., Fink, G. R., Amunts, K., & Zilles, K. (2005). A new SPM toolbox for combining probabilistic cytoarchitectonic maps and functional imaging data. *NeuroImage*, 25(4), 1325–1335. <https://doi.org/10.1016/j.neuroimage.2004.12.034>, PubMed: 15850749
- Farahani, F. V., Karwowski, W., & Lighthall, N. R. (2019). Application of graph theory for identifying connectivity patterns in human brain networks: A systematic review. *Frontiers in Neuroscience*, 13, 585. <https://doi.org/10.3389/fnins.2019.00585>, PubMed: 31249501
- Freeman, L. C. (1979). Centrality in social networks conceptual clarification. *Social Networks*, 1(3), 215–239. [https://doi.org/10.1016/0378-8733\(78\)90021-7](https://doi.org/10.1016/0378-8733(78)90021-7)
- Friederici, A. D., & Gierhan, S. M. (2013). The language network. *Current Opinion in Neurobiology*, 23(2), 250–254. <https://doi.org/10.1016/j.conb.2012.10.002>, PubMed: 23146876
- Genon, S., Li, H., Fan, L., Müller, V. I., Cieslik, E. C., Hoffstaedter, F., ... Eickhoff, S. B. (2017). The right dorsal premotor mosaic: Organization, functions, and connectivity. *Cerebral Cortex*, 27(3), 2095–2110. <https://doi.org/10.1093/cercor/bhw065>, PubMed: 26965906
- Gillebert, C. R., Mantini, D., Peeters, R., Dupont, P., & Vandenberghe, R. (2013). Cytoarchitectonic mapping of attentional selection and reorienting in parietal cortex. *NeuroImage*, 67, 257–272. <https://doi.org/10.1016/j.neuroimage.2012.11.026>, PubMed: 23201362
- Girard, G., Caminiti, R., Battaglia-Mayer, A., St-Onge, E., Ambrosen, K. S., Eskildsen, S. F., ... Innocenti, G. M. (2020). On the cortical connectivity in the macaque brain: A comparison of diffusion tractography and histological tracing data. *NeuroImage*, 221, 117201. <https://doi.org/10.1016/j.neuroimage.2020.117201>, PubMed: 32739552
- Gong, G., He, Y., Concha, L., Lebel, C., Gross, D. W., Evans, A. C., & Beaulieu, C. (2009). Mapping anatomical connectivity patterns of human cerebral cortex using in vivo diffusion tensor imaging tractography. *Cerebral Cortex*, 19(3), 524–536. <https://doi.org/10.1093/cercor/bhn102>, PubMed: 18567609
- Goodale, M. A., & Milner, A. D. (1992). Separate visual pathways for perception and action. *Trends in Neurosciences*, 15(1), 20–25. [https://doi.org/10.1016/0166-2236\(92\)90344-8](https://doi.org/10.1016/0166-2236(92)90344-8), PubMed: 1374953
- Greulich, R. S., Adam, R., Everling, S., & Scherberger, H. (2020). Shared functional connectivity between the dorso-medial and dorso-ventral streams in macaques. *Scientific Reports*, 10(1), 18610. <https://doi.org/10.1038/s41598-020-75219-x>, PubMed: 33122655
- Guimerà, R., & Nunes Amaral, L. A. (2005). Functional cartography of complex metabolic networks. *Nature*, 433(7028), 895–900. <https://doi.org/10.1038/nature03288>, PubMed: 15729348
- Hemmerich, W. (2016). *StatistikGuru: Rechner zur adjustierung des α -niveaus*. <https://statistikguru.de/rechner/adjustierung-des-alpha-niveaus.html>
- Hernández, M., Guerrero, G. D., Cecilia, J. M., García, J. M., Inuggi, A., Jbabdi, S., ... Sotiropoulos, S. N. (2013). Accelerating fibre orientation estimation from diffusion weighted magnetic resonance imaging using GPUs. *PLOS ONE*, 8(4), e61892. <https://doi.org/10.1371/journal.pone.0061892>, PubMed: 23658616
- Hertrich, I., Dietrich, S., & Ackermann, H. (2016). The role of the supplementary motor area for speech and language processing. *Neuroscience & Biobehavioral Reviews*, 68, 602–610. <https://doi.org/10.1016/j.neubiorev.2016.06.030>, PubMed: 27343998
- Hesling, I., Labache, L., Joliot, M., & Tzourio-Mazoyer, N. (2019). Large-scale plurimodal networks common to listening to, producing and reading word lists: An fMRI study combining task-induced activation and intrinsic connectivity in 144 right-handers. *Brain Structure & Function*, 224(9), 3075–3094. <https://doi.org/10.1007/s00429-019-01951-4>, PubMed: 31494717
- Humphries, M. D., & Gurney, K. (2008). Network 'small-world-ness': A quantitative method for determining canonical network equivalence. *PLOS ONE*, 3(4), e0002051. <https://doi.org/10.1371/journal.pone.0002051>, PubMed: 18446219
- Jbabdi, S., Sotiropoulos, S. N., Savio, A. M., Graña, M., & Behrens, T. E. J. (2012). Model-based analysis of multishell diffusion MR data for tractography: How to get over fitting problems. *Magnetic Resonance in Medicine*, 68(6), 1846–1855. <https://doi.org/10.1002/mrm.24204>, PubMed: 22334356
- Jeannerod, M., Arbib, M. A., Rizzolatti, G., & Sakata, H. (1995). Grasping objects: The cortical mechanisms of visuomotor transformation. *Trends in Neurosciences*, 18(7), 314–320. [https://doi.org/10.1016/0166-2236\(95\)93921-J](https://doi.org/10.1016/0166-2236(95)93921-J), PubMed: 7571012
- Jenkinson, M., Bannister, P., Brady, M., & Smith, S. (2002). Improved optimization for the robust and accurate linear registration and motion correction of brain images. *NeuroImage*, 17(2), 825–841. <https://doi.org/10.1006/nimg.2002.1132>, PubMed: 12377157
- Jenkinson, M., & Smith, S. (2001). A global optimisation method for robust affine registration of brain images. *Medical Image Analysis*, 5(2), 143–156. [https://doi.org/10.1016/S1361-8415\(01\)00036-6](https://doi.org/10.1016/S1361-8415(01)00036-6), PubMed: 11516708
- Jiang, X., Zhao, L., Liu, H., Guo, L., Kendrick, K. M., & Liu, T. (2018). A cortical folding pattern-guided model of intrinsic functional brain networks in emotion processing. *Frontiers in Neuroscience*, 12, 575. <https://doi.org/10.3389/fnins.2018.00575>, PubMed: 30186102
- Jung, J., Cloutman, L. L., Binney, R. J., & Lambon Ralph, M. A. (2017). The structural connectivity of higher order association cortices reflects human functional brain networks. *Cortex*, 97, 221–239. <https://doi.org/10.1016/j.cortex.2016.08.011>, PubMed: 27692846
- Jung, J., Visser, M., Binney, R. J., & Lambon Ralph, M. A. (2018). Establishing the cognitive signature of human brain networks derived from structural and functional connectivity. *Brain Structure & Function*, 223(9), 4023–4038. <https://doi.org/10.1007/s00429-018-1734-x>, PubMed: 30120553
- Karnath, H.-O., & Perenin, M.-T. (2005). Cortical control of visually guided reaching: Evidence from patients with optic ataxia. *Cerebral Cortex*, 15(10), 1561–1569. <https://doi.org/10.1093/cercor/bhi034>, PubMed: 15716470
- Konen, C. S., Mruczek, R. E. B., Montoya, J. L., & Kastner, S. (2013). Functional organization of human posterior parietal cortex:

- Grasping- and reaching-related activations relative to topographically organized cortex. *Journal of Neurophysiology*, 109(12), 2897–2908. <https://doi.org/10.1152/jn.00657.2012>, PubMed: 23515795
- Liu, T., & Pleskac, T. J. (2011). Neural correlates of evidence accumulation in a perceptual decision task. *Journal of Neurophysiology*, 106(5), 2383–2398. <https://doi.org/10.1152/jn.00413.2011>, PubMed: 21849612
- Madhavan, A., Schwarz, C. G., Duffy, J. R., Strand, E. A., Machulda, M. M., Drubach, D. A., ... Whitwell, J. L. (2016). Characterizing white matter tract degeneration in syndromic variants of Alzheimer's disease: A diffusion tensor imaging study. *Journal of Alzheimer's Disease*, 49(3), 633–643. <https://doi.org/10.3233/JAD-150502>, PubMed: 26484918
- Mars, R. B., Jbabdi, S., Sallet, J., O'Reilly, J. X., Croxson, P. L., Olivier, E., ... Rushworth, M. F. S. (2011). Diffusion-weighted imaging tractography-based parcellation of the human parietal cortex and comparison with human and macaque resting-state functional connectivity. *Journal of Neuroscience*, 31(11), 4087–4100. <https://doi.org/10.1523/JNEUROSCI.5102-10.2011>, PubMed: 21411650
- Meunier, D., Lambiotte, R., Fornito, A., Ersche, K. D., & Bullmore, E. T. (2009). Hierarchical modularity in human brain functional networks. *Frontiers in Neuroinformatics*, 3, 37. <https://doi.org/10.3389/neuro.11.037.2009>, PubMed: 19949480
- Mishkin, M., & Ungerleider, L. G. (1982). Contribution of striate inputs to the visuospatial functions of parieto-preoccipital cortex in monkeys. *Behavioural Brain Research*, 6(1), 57–77. [https://doi.org/10.1016/0166-4328\(82\)90081-X](https://doi.org/10.1016/0166-4328(82)90081-X), PubMed: 7126325
- Nachev, P., Kennard, C., & Husain, M. (2008). Functional role of the supplementary and pre-supplementary motor areas. *Nature Reviews Neuroscience*, 9(11), 856–869. <https://doi.org/10.1038/nrn2478>, PubMed: 18843271
- Newman, M. E. J. (2006). Finding community structure in networks using the eigenvectors of matrices. *Physical Review E*, 74(3 Pt 2), 036104. <https://doi.org/10.1103/PhysRevE.74.036104>, PubMed: 17025705
- Nuttall, H. E., Kennedy-Higgins, D., Devlin, J. T., & Adank, P. (2018). Modulation of intra- and inter-hemispheric connectivity between primary and premotor cortex during speech perception. *Brain and Language*, 187, 74–82. <https://doi.org/10.1016/j.bandl.2017.12.002>, PubMed: 29397191
- Orban, G. A., & Caruana, F. (2014). The neural basis of human tool use. *Frontiers in Psychology*, 5, 310. <https://doi.org/10.3389/fpsyg.2014.00310>, PubMed: 24782809
- Orban, G. A., Claeys, K., Nelissen, K., Smans, R., Sunaert, S., Todd, J. T., ... Vanduffel, W. (2006). Mapping the parietal cortex of human and non-human primates. *Neuropsychologia*, 44(13), 2647–2667. <https://doi.org/10.1016/j.neuropsychologia.2005.11.001>, PubMed: 16343560
- Passingham, R. (2008). *What is special about the human brain?* Oxford University Press. <https://doi.org/10.1093/acprof:oso/9780199230136.001.0001>
- Passingham, R. E., & Lau, H. C. (2019). Acting, seeing, and conscious awareness. *Neuropsychologia*, 128, 241–248. <https://doi.org/10.1016/j.neuropsychologia.2017.06.012>, PubMed: 28623108
- Passingham, R. E., Stephan, K. E., & Kötter, R. (2002). The anatomical basis of functional localization in the cortex. *Nature Reviews Neuroscience*, 3(8), 606–616. <https://doi.org/10.1038/nrn893>, PubMed: 12154362
- Pisella, L., Binkofski, F., Lasek, K., Toni, I., & Rossetti, Y. (2006). No double-dissociation between optic ataxia and visual agnosia: Multiple sub-streams for multiple visuo-manual integrations. *Neuropsychologia*, 44(13), 2734–2748. <https://doi.org/10.1016/j.neuropsychologia.2006.03.027>, PubMed: 16753188
- Pitcher, D., & Ungerleider, L. G. (2021). Evidence for a third visual pathway specialized for social perception. *Trends in Cognitive Sciences*, 25(2), 100–110. <https://doi.org/10.1016/j.tics.2020.11.006>, PubMed: 33334693
- Ramayya, A. G., Glasser, M. F., & Rilling, J. K. (2010). A DTI investigation of neural substrates supporting tool use. *Cerebral Cortex*, 20(3), 507–516. <https://doi.org/10.1093/cercor/bhp141>, PubMed: 19608779
- Richter, M., Amunts, K., Mohlberg, H., Bludau, S., Eickhoff, S. B., Zilles, K., & Caspers, S. (2019). Cytoarchitectonic segregation of human posterior intraparietal and adjacent parieto-occipital sulcus and its relation to visuomotor and cognitive functions. *Cerebral Cortex*, 29(3), 1305–1327. <https://doi.org/10.1093/cercor/bhy245>, PubMed: 30561508
- Rizzolatti, G., & Craighero, L. (2004). The mirror-neuron system. *Annual Review of Neuroscience*, 27, 169–192. <https://doi.org/10.1146/annurev.neuro.27.070203.144230>, PubMed: 15217330
- Rizzolatti, G., & Luppino, G. (2001). The cortical motor system. *Neuron*, 31(6), 889–901. [https://doi.org/10.1016/S0896-6273\(01\)00423-8](https://doi.org/10.1016/S0896-6273(01)00423-8), PubMed: 11580891
- Rizzolatti, G., Luppino, G., & Matelli, M. (1998). The organization of the cortical motor system: New concepts. *Electroencephalography and Clinical Neurophysiology*, 106(4), 283–296. [https://doi.org/10.1016/S0013-4694\(98\)00022-4](https://doi.org/10.1016/S0013-4694(98)00022-4), PubMed: 9741757
- Rizzolatti, G., & Matelli, M. (2003). Two different streams form the dorsal visual system: Anatomy and functions. *Experimental Brain Research*, 153(2), 146–157. <https://doi.org/10.1007/s00221-003-1588-0>, PubMed: 14610633
- Rodríguez-Herreros, B., Amengual, J. L., Gurtubay-Antolín, A., Richter, L., Jauer, P., Erdmann, C., ... Münte, T. F. (2015). Microstructure of the superior longitudinal fasciculus predicts stimulation-induced interference with on-line motor control. *NeuroImage*, 120, 254–265. <https://doi.org/10.1016/j.neuroimage.2015.06.070>, PubMed: 26143205
- Roski, C., Caspers, S., Langner, R., Laird, A. R., Fox, P. T., Zilles, K., ... Eickhoff, S. B. (2013). Adult age-dependent differences in resting-state connectivity within and between visual-attention and sensorimotor networks. *Frontiers in Aging Neuroscience*, 5, 67. <https://doi.org/10.3389/fnagi.2013.00067>, PubMed: 24194718
- Rottschy, C., Langner, R., Dogan, I., Reetz, K., Laird, A. R., Schulz, J. B., ... Eickhoff, S. B. (2012). Modelling neural correlates of working memory: A coordinate-based meta-analysis. *NeuroImage*, 60(1), 830–846. <https://doi.org/10.1016/j.neuroimage.2011.11.050>, PubMed: 22178808
- Rubinov, M., & Sporns, O. (2010). Complex network measures of brain connectivity: Uses and interpretations. *NeuroImage*, 52(3), 1059–1069. <https://doi.org/10.1016/j.neuroimage.2009.10.003>, PubMed: 19819337
- Sakreida, K., Effner, I., Thill, S., Menz, M. M., Jirak, D., Eickhoff, C. R., ... Binkofski, F. (2016). Affordance processing in segregated

- parieto-frontal dorsal stream sub-pathways. *Neuroscience and Biobehavioral Reviews*, 69, 89–112. <https://doi.org/10.1016/j.neubiorev.2016.07.032>, PubMed: 27484872
- Saur, D., Kreher, B. W., Schnell, S., Kümmerer, D., Kellmeyer, P., Vry, M.-S., ... Weiller, C. (2008). Ventral and dorsal pathways for language. *Proceedings of the National Academy of Sciences of the United States of America*, 105(46), 18035–18040. <https://doi.org/10.1073/pnas.0805234105>, PubMed: 19004769
- Schilling, K., Gao, Y., Janve, V., Stepniewska, I., Landman, B. A., & Anderson, A. W. (2018). Confirmation of a gyral bias in diffusion MRI fiber tractography. *Human Brain Mapping*, 39(3), 1449–1466. <https://doi.org/10.1002/hbm.23936>, PubMed: 29266522
- Smith, S. M. (2002). Fast robust automated brain extraction. *Human Brain Mapping*, 17(3), 143–155. <https://doi.org/10.1002/hbm.10062>, PubMed: 12391568
- Smith, S. M., Jenkinson, M., Woolrich, M. W., Beckmann, C. F., Behrens, T. E. J., Johansen-Berg, H., ... Matthews, P. M. (2004). Advances in functional and structural MR image analysis and implementation as FSL. *NeuroImage*, 23(Suppl. 1), S208–S219. <https://doi.org/10.1016/j.neuroimage.2004.07.051>, PubMed: 15501092
- Sotiropoulos, S. N., Hernández-Fernández, M., Vu, A. T., Andersson, J. L., Moeller, S., Yacoub, E., ... Jbabdi, S. (2016). Fusion in diffusion MRI for improved fibre orientation estimation: An application to the 3T and 7T data of the Human Connectome Project. *NeuroImage*, 134, 396–409. <https://doi.org/10.1016/j.neuroimage.2016.04.014>, PubMed: 27071694
- Sporns, O., Honey, C. J., & Kötter, R. (2007). Identification and classification of hubs in brain networks. *PLoS One*, 2(10), e1049. <https://doi.org/10.1371/journal.pone.0001049>, PubMed: 17940613
- Thiebaut de Schotten, M., Dell’Acqua, F., Forkel, S. J., Simmons, A., Vergani, F., Murphy, D. G. M., & Catani, M. (2011). A lateralized brain network for visuospatial attention. *Nature Neuroscience*, 14(10), 1245–1246. <https://doi.org/10.1038/nn.2905>, PubMed: 21926985
- Thiebaut de Schotten, M., Ffytche, D. H., Bizzi, A., Dell’Acqua, F., Allin, M., Walshe, M., ... Catani, M. (2011). Atlasing location, asymmetry and inter-subject variability of white matter tracts in the human brain with MR diffusion tractography. *NeuroImage*, 54(1), 49–59. <https://doi.org/10.1016/j.neuroimage.2010.07.055>, PubMed: 20682348
- Tomassini, V., Jbabdi, S., Klein, J. C., Behrens, T. E. J., Pozzilli, C., Matthews, P. M., ... Johansen-Berg, H. (2007). Diffusion-weighted imaging tractography-based parcellation of the human lateral premotor cortex identifies dorsal and ventral subregions with anatomical and functional specializations. *Journal of Neuroscience*, 27(38), 10259–10269. <https://doi.org/10.1523/JNEUROSCI.2144-07.2007>, PubMed: 17881532
- Tournier, J.-D., Mori, S., & Leemans, A. (2011). Diffusion tensor imaging and beyond. *Magnetic Resonance in Medicine*, 65(6), 1532–1556. <https://doi.org/10.1002/mrm.22924>, PubMed: 21469191
- Tsai, S.-Y. (2018). Reproducibility of structural brain connectivity and network metrics using probabilistic diffusion tractography. *Scientific Reports*, 8(1), 11562. <https://doi.org/10.1038/s41598-018-29943-0>, PubMed: 30068926
- Uddin, L. Q., Supekar, K., Amin, H., Rykhlevskaia, E., Nguyen, D. A., Greicius, M. D., & Menon, V. (2010). Dissociable connectivity within human angular gyrus and intraparietal sulcus: Evidence from functional and structural connectivity. *Cerebral Cortex*, 20(11), 2636–2646. <https://doi.org/10.1093/cercor/bhq011>, PubMed: 20154013
- Uehara, T., Yamasaki, T., Okamoto, T., Koike, T., Kan, S., Miyauchi, S., ... Tobimatsu, S. (2014). Efficiency of a “small-world” brain network depends on consciousness level: A resting-state fMRI study. *Cerebral Cortex*, 24(6), 1529–1539. <https://doi.org/10.1093/cercor/bht004>, PubMed: 23349223
- Urbanski, M., Thiebaut de Schotten, M., Rodrigo, S., Catani, M., Oppenheim, C., Touzé, E., ... Bartolomeo, P. (2008). Brain networks of spatial awareness: Evidence from diffusion tensor imaging tractography. *Journal of Neurology, Neurosurgery, and Psychiatry*, 79(5), 598–601. <https://doi.org/10.1136/jnnp.2007.126276>, PubMed: 17991702
- Van Doren, L., Dupont, P., De Grauwe, S., Peeters, R., & Vandenberghe, R. (2010). The amodal system for conscious word and picture identification in the absence of a semantic task. *NeuroImage*, 49(4), 3295–3307. <https://doi.org/10.1016/j.neuroimage.2009.12.005>, PubMed: 20004724
- Verhagen, L., Dijkerman, H. C., Medendorp, W. P., & Toni, I. (2013). Hierarchical organization of parietofrontal circuits during goal-directed action. *Journal of Neuroscience*, 33(15), 6492–6503. <https://doi.org/10.1523/JNEUROSCI.3928-12.2013>, PubMed: 23575847
- Watts, D. J., & Strogatz, S. H. (1998). Collective dynamics of ‘small-world’ networks. *Nature*, 393(6684), 440–442. <https://doi.org/10.1038/30918>, PubMed: 9623998
- Xia, M., Wang, J., & He, Y. (2013). BrainNet viewer: A network visualization tool for human brain connectomics. *PLOS ONE*, 8(7), e68910. <https://doi.org/10.1371/journal.pone.0068910>, PubMed: 23861951
- Yeh, C.-H., Jones, D. K., Liang, X., Descoteaux, M., & Connelly, A. (2021). Mapping structural connectivity using diffusion MRI: Challenges and opportunities. *Journal of Magnetic Resonance Imaging*, 53(6), 1666–1682. <https://doi.org/10.1002/jmri.27188>, PubMed: 32557893
- Yun, J.-Y., Boedhoe, P. S. W., Vriend, C., Jahanshad, N., Abe, Y., Ameis, S. H., ... Kwon, J. S. (2020). Brain structural covariance networks in obsessive-compulsive disorder: A graph analysis from the ENIGMA Consortium. *Brain*, 143(2), 684–700. <https://doi.org/10.1093/brain/awaa001>, PubMed: 32040561
- Zanto, T. P., Rubens, M. T., Bollinger, J., & Gazzaley, A. (2010). Top-down modulation of visual feature processing: The role of the inferior frontal junction. *NeuroImage*, 53(2), 736–745. <https://doi.org/10.1016/j.neuroimage.2010.06.012>, PubMed: 20600999
- Zhang, Y., Wang, Y., Chen, N., Guo, M., Wang, X., Chen, G., ... Hu, B. (2021). Age-associated differences of modules and hubs in brain functional networks. *Frontiers in Aging Neuroscience*, 12, 607445. <https://doi.org/10.3389/fnagi.2020.607445>, PubMed: 33536893